ELSEVIER

Contents lists available at ScienceDirect

Ocean Engineering

journal homepage: www.elsevier.com/locate/oceaneng



Research paper

A calculation method for the digital twin of aging jacket platforms within the digital healthcare engineering framework

Keyang Liu ^a, Yuanchang Liu ^a, Baoping Cai ^b, Jeom Kee Paik ^{a,c,d,*}

- ^a Department of Mechanical Engineering, University College London, London, UK
- ^b College of Mechanical and Electronic Engineering, China University of Petroleum, Qingdao, Shandong, 266580, China
- ^c Faculty of Maritime and Transportation, Ningbo University, Ningbo, China
- ^d Hangzhou City University Binjiang Innovation Center, Hangzhou, China

ARTICLE INFO

Keywords:
Aging jacket platforms
Digital healthcare engineering (DHE)
Digital twin
Residual ultimate strength
Environmental load

ABSTRACT

Offshore jacket platforms operate for extended periods in harsh marine environments, during which a series of aging-related defects may occur in their structures, leading to reduced load-bearing capacity. Efficient computation of environmental loads and residual ultimate strength, enabling real-time monitoring of safety levels, is critical to ensuring their safe operation. However, existing computational methods suffer from systemic weaknesses and low efficiency, and there is also a lack of effective approaches for analyzing defects in aging structures. To address these issues, A calculation method for the digital twin of aging jacket platforms within the Digital Healthcare Engineering (DHE) framework is proposed, aimed at enabling efficient analysis of environmental and defect parameters obtained from on-site measurements. Specifically, an environmental load computation framework is established based on surrogate models, Morison equation, and wave theories, while a residual ultimate strength computation framework is developed using multi-scale finite element models, nonlinear finite element analysis, and structural defect simulation methods. This approach forms a standardized analytical workflow that balances computational accuracy and efficiency, reduces computation time, and enables effective analysis of monitoring data. The effectiveness of the proposed method is validated using a case study of a specific jacket platform.

1. Introduction

Jacket platforms play a crucial role in offshore oil and gas development(Zheng et al., 2024). Many platforms remain in operation even after reaching their design service life. As the service period extends, the aging of jacket platforms becomes increasingly prominent. Extending the operational life of these platforms can significantly enhance the economic efficiency of resource development(Huang et al., 2025). However, the combination of harsh marine environments and structural aging also poses substantial risks and challenges to operational safety. Implementing effective structural monitoring and health management for aging jacket platforms is a key measure to ensure their safe operation (Wahab et al., 2020).

However, the existing structural health management methods for aging jacket platforms are characterized by poor real-time performance and low levels of digitization and intelligence. In particular, when faced with complex and severe marine environments, such as storms, it is

difficult to achieve real-time and accurate safety assessment and decision-making(Fadzil et al., 2024). To address these issues, Paik (2024) proposed the concept of Digital Healthcare Engineering (DHE), providing a comprehensive solution for the health management of aging offshore structures. This concept enables real-time health assessment and decision-making by leveraging digital technologies, communication systems, and artificial intelligence.

DHE comprises five interrelated modules(Sindi et al., 2025): (1) In-situ measurements of health parameters; (2) Data transmission and communication; (3) Data analytics and visualization with digital twins; (4) AI-based diagnosis and remedial action recommendations; and (5) Prediction of future health conditions. The conceptual model of DHE is shown in Fig. 1.

In Module 1, the information that needs to be collected on-site primarily includes two aspects: environmental parameters and structural defect parameters. Through real-time monitoring and periodic manual inspections, timely acquisition and updating of on-site information are

^{*} Corresponding author. Department of Mechanical Engineering, University College London, London, UK.

E-mail addresses: keyang.liu.24@ucl.ac.uk (K. Liu), yuanchang.liu@ucl.ac.uk (Y. Liu), caibaoping@upc.edu.cn (B. Cai), j.paik@ucl.ac.uk (J.K. Paik).

achieved. Module 2 uses communication technologies, such as low Earth orbit satellites, to transmit the on-site information to the digital analysis platform. Module 3 establishes a digital twin computational model to analyze the on-site data. Modules 4 and 5, based on the computational results, further provide health diagnostics, maintenance, and predictive schemes, and feed the results back to the field to support decisionmaking. In this way, DHE establishes a real-time, bidirectional connection between the field and the analysis platform, with a feedback mechanism, enabling digital twin-driven structural health management. Currently, this concept has been preliminarily explored in aging ships and structures(Sindi et al., 2024), offshore wind turbine foundations(Xie et al., 2025), LNG storage tanks(Duan et al., 2024), and crew health management(Cui et al., 2025). This work focuses on Module 3, primarily developing the digital twin model to analyze on-site data for computing environmental loads and the residual ultimate strength of the aging jacket platform.

The digital twin model needs to be dynamically and timely updated in accordance with the changes of the physical entity (Lee et al., 2022). Achieving real-time, rapid computation while ensuring calculation accuracy is the core task of a digital twin model and serves as a key criterion for evaluating its success(Wang et al., 2024). To this end, numerous studies have conducted preliminary explorations. Currently, digital twin modeling approaches can be categorized into physics-based modeling and data-driven modeling. Kim and Paik (2025) using the MAESTRO software, implemented fast finite element analysis and developed a digital twin model for aging container ships, enabling real-time updates of wave loads and hull structural ultimate strength. Jayasinghe et al. (2024) trained artificial neural networks on data generated from finite element models to establish a digital twin of port structures, achieving rapid predictions of structural responses. Data-driven models offer advantages in real-time performance and do not require explicit physical mechanisms, but they rely heavily on high-quality data(Zou et al., 2024), which is often difficult to obtain in practice. Physics-based modeling, on the other hand, provides strong interpretability and flexibility but involves higher modeling costs and computational complexity(Westin and A. Irani, 2025). When modeling complex systems, relying solely on one approach often fails to meet practical needs. Developing a customized digital twin approach for aging jacket platforms, establishing a standardized analysis workflow, and implementing the computation of environmental loads and residual ultimate strength while balancing computational accuracy and efficiency—are essential for realizing an effective digital twin.

In the computation of environmental loads on jacket platforms,

wind, waves, and ocean currents are the three most common and dominant load types. Among these, wind loads primarily act on the topside modules, generating significant horizontal thrust under high wind speeds. Under extreme conditions such as typhoons, wind loads can even directly cause lateral displacement or failure of the topside structure. Currently, wind load calculations primarily rely on drag force formulas recommended by industry standards such as the API(Tian et al., 2019). Although these methods are simple and enable rapid computation, they neglect the effects of turbulence intensity in the wind, aerodynamic interactions among topside modules, and shielding effects between different modules(Liu et al., 2021). The shape coefficients recommended in the standards are only provided for simple structures, making it difficult to apply them to facilities with complex configurations, and they do not reflect variations with wind direction. While CFD methods can provide accurate calculations of wind loads, they require large computational resources and are inefficient(Lin et al., 2025), making them unsuitable for the needs of digital twin models. For hydrodynamic load calculations, the Morrison equation offers an accurate and efficient method for computing wave and current loads and is the primary approach used in current research(Liang et al., 2022). When applying this method, it is necessary to select an appropriate wave theory based on actual environmental parameters and to specify the ocean current velocity profile. Especially under extreme conditions such as storms, waves exhibit pronounced nonlinear characteristics and significantly increased wave heights, resulting in more concentrated loads. High-order wave theories should be employed in calculations to capture the nonlinear behavior of waves(Raheem, 2014).

The residual ultimate strength represents the maximum load that a jacket platform can withstand under its current damaged condition and serves as a critical criterion for determining whether the structure is fit for continued service(Othman and Mohd, 2024). Through proper assessment, structural vulnerabilities can be identified, and potential failure modes predicted, thereby helping to prevent major safety incidents(Yang et al., 2019). Nonlinear pushover analysis (Pushover) is a key method for evaluating the ultimate strength of jacket platforms (Karimi et al., 2017) and is widely applied in the life-extension assessment and collapse resistance studies of aging offshore structures (Asgarian et al., 2019).

In pushover analysis, nonlinear finite element analysis is involved. At the same time, structural defects such as corrosion(Bai et al., 2016), fatigue cracking (Ali et al., 2021), and mechanical denting(Zhu et al., 2020) also need to be simulated, resulting in a typically very large computational demand. Although analyzing jacket platforms using

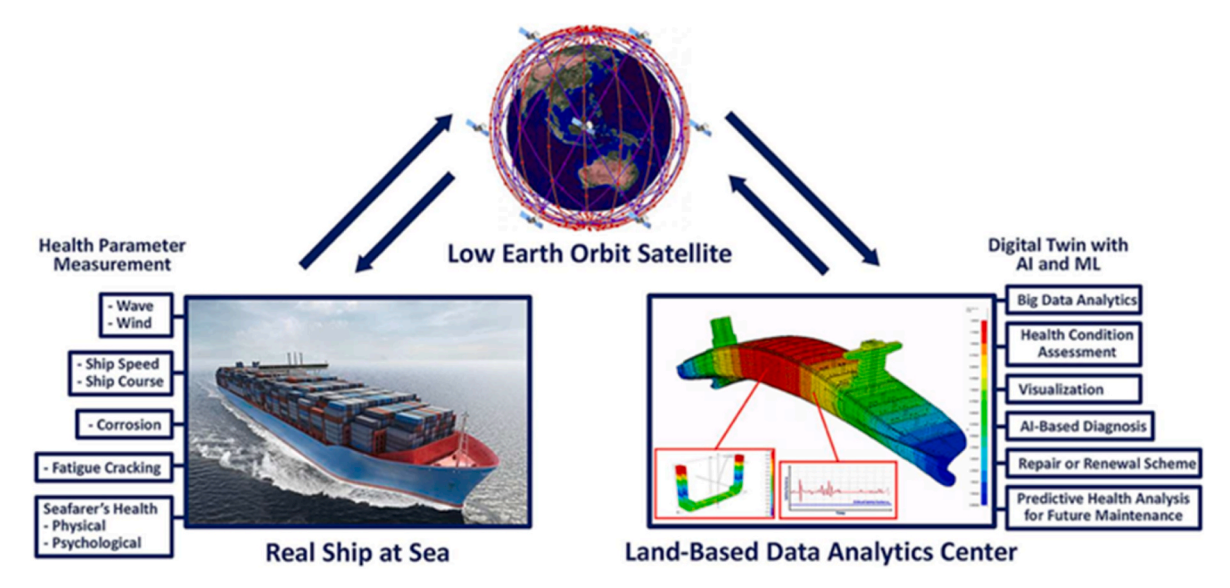


Fig. 1. Digital healthcare engineering for aging offshore structures (Paik, 2024).

macroscopically simplified frame elements can reflect the overall structural performance while simplifying calculations and improving efficiency(Zhou et al., 2014), it is difficult to incorporate local defects and capture the microscopic mechanisms of local damage. Conversely, modeling the platform using microscopic or local-scale finite elements allows structural defects to be easily introduced(Tabeshpour et al., 2020), but this approach dramatically increases the number of elements, reduces computational efficiency, and may even make the problem intractable. In practical engineering, computational resources are limited, and safety assessments of aging jacket platforms often face tight decision-making time windows. The computational efficiency of a numerical model directly determines whether the analysis method is viable in engineering applications.

Multiscale finite element analysis provides a reasonable solution to this issue. The core idea of multiscale finite element analysis is to capture the macroscopic response at the global structural level while introducing higher-resolution detailed modeling in local critical regions, thereby achieving an organic combination of accuracy and efficiency (Ruan et al., 2023). Multiscale finite element models can be divided into three levels. The macroscopic-scale model is used for overall structural modeling and pushover path analysis. The microscopic-scale finite element model is employed to simulate critical regions where aging defects occur, in order to capture local responses. Additionally, coupling relationships must be established between elements at different scales to achieve coordinated overall solutions. Leng et al. (2025) applied the multiscale modeling concept to develop a detailed model for splash-zone

tubular joints, while simulating other components using macroscopic elements, reducing model complexity and enabling the simulation of crack propagation. Lin et al. (2022) introduced an element-coupling method to establish a jacket platform analysis model under ship collision, significantly reducing modeling and computational costs, and efficiently conducting numerical analysis of failure modes and collision processes.

However, current multiscale finite element modeling and scale-coupling methods remain inconsistent, and standardized methods for simulating structural defects are lacking. In the interface regions of multiscale models, information discontinuities often occur, affecting the smoothness and convergence of the overall solution. Local regions of multiscale models involve complex stress states and nonlinear responses, inevitably introducing errors (Chiu and Yu, 2023). Whether a model can achieve coordinated global solution and successfully incorporate microscopic defects into the overall model to assist in computing residual ultimate strength still requires further validation.

To address the aforementioned issues, this work proposes a calculation method for the digital twin model of aging jacket platforms within the DHE framework. Based on surrogate models, the Morison equation, and wave theory, the approach enables near real-time calculation of wind, wave, and current loads. A detailed modeling and description method for aging structural defects is presented, analyzing defects such as corrosion, cracks, and dents. A multiscale finite element model is employed to incorporate local defects into the overall structure, facilitating the computation of residual ultimate strength and achieving a

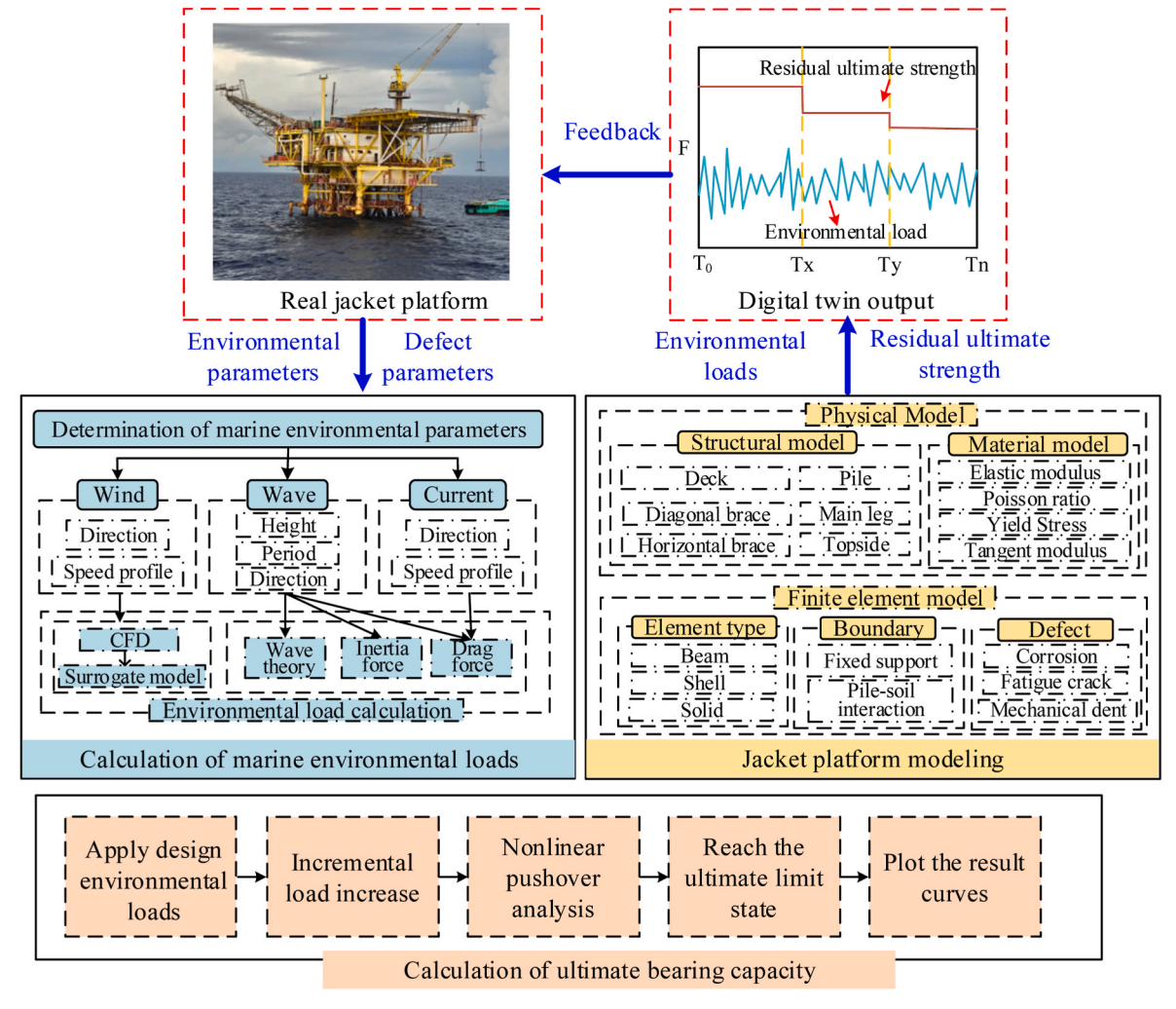


Fig. 2. The proposed method.

balance between computational accuracy and efficiency.

The remainder of this paper is organized as follows. Section 2 elaborates on the proposed methodology. Section 3 presents a computational validation using a specific jacket platform as a case study. Section 4 concludes the paper.

2. The proposed method

The proposed digital twin calculation method for aging jacket platforms primarily consists of four components: environmental load calculation, aging jacket platform modeling, residual ultimate strength calculation, and digital twin–driven health monitoring, as shown in Fig. 2.

The first component is environmental load calculation, which involves computing the loads acting on the jacket platform, including wind, waves, and currents. For wind load calculation, considering the issues with standard codes—such as the recommended coefficients being applicable only to simple structures, the lack of variation with wind direction, difficulty in accurately estimating the windward area of upper modules, and the high computational cost of CFD—a Kriging surrogate model is proposed to achieve accurate and rapid wind load computation. Wave and current loads are calculated based on the Morison equation, combined with wave theory and current velocity profiles.

The second component is modeling of the aging jacket platform. A multi-element hybrid modeling strategy is adopted to establish an overall model including the topside modules, jacket, and piles. A multi-scale modeling approach is employed, with constraint equations applied at connections between different-scale elements to achieve coupling. Local detailed defect models are introduced within the global structure to simulate corrosion, cracks, and dents, improving computational efficiency while maintaining accuracy.

The third component is ultimate strength calculation. Using pushover analysis, environmental loads are incrementally increased to determine the structure's ultimate load-bearing capacity.

The fourth component is digital twin-driven structural health monitoring. By continuously acquiring in-situ parameters, environmental loads and residual ultimate strength are updated, enabling near real-time health monitoring, with the analysis results fed back to the field.

The primary objective of this study is to develop a computational method within the DHE framework to support the digital twin model of aging jacket platforms. Within the DHE framework, the primary task of the digital twin model is to efficiently analyze environmental parameters and structural defect parameters, thereby enabling the calculation of environmental loads and residual ultimate strength. Based on these calculations, safety factors can be updated to assess structural safety and to support further structural analyses. Therefore, the calculation of environmental loads and residual ultimate strength is a critical issue that must be addressed by the digital twin model, and it constitutes the main focus of this study.

2.1. Calculation of environmental loads

The environmental loads acting on a jacket platform can be broadly classified into two categories: aerodynamic loads and hydrodynamic loads. Aerodynamic loads refer to wind loads acting on the topside modules, while hydrodynamic loads include wave and current forces acting below the sea surface.

2.1.1. Wind load

The proposed wind load calculation method mainly consists of four steps: sample point generation, CFD computation, surrogate model construction, and wind load prediction.

(1) Sample point generation

The main task of this step is to perform reasonable sampling within the range of the independent variables to generate sample points, which will support the subsequent training and tuning of the surrogate model. Wind direction and wind speed are selected as the independent variables, with their respective ranges defined by Eqs (1) and (2).

$$V \in [0, V_{\text{max}}] \tag{1}$$

$$Direction \in [0^{\circ}, 360^{\circ}] \tag{2}$$

where, V_{max} denotes the maximum possible wind speed, which can correspond to the 100-year return period wind speed or a value higher than that.

Within the range of the variables, a reasonable sampling method can be used to select sample points; for example, Latin Hypercube Sampling (LHS) can be employed.

(2) Numerical simulation based on CFD

The main task in this step is to perform CFD calculations at each sample point for the corresponding wind speed and direction, in order to obtain accurate wind load values and generate a complete dataset for training the surrogate model.

The principle of CFD analysis involves discretizing the governing equations of fluid motion using numerical methods to solve for the distributions of velocity, pressure, temperature, and other flow field variables, thereby enabling the analysis of fluid behavior and the resulting forces. The governing equations include the continuity equation, the Navier–Stokes equations, and the law of conservation of energy, as shown in Eqs (3)–(5).

$$\frac{\partial \rho}{\partial t} + \nabla \cdot (\rho \, \overrightarrow{u}) = 0 \tag{3}$$

$$\rho\left(\frac{\partial \overrightarrow{u}}{\partial t} + \overrightarrow{u} \cdot \nabla \overrightarrow{u}\right) = -\nabla p + \mu \nabla^2 \overrightarrow{u} + \overrightarrow{f}$$
(4)

$$\rho c_p \left(\frac{\partial T}{\partial t} + \overrightarrow{u} \cdot \nabla T \right) = k \nabla^2 T + Q \tag{5}$$

where, ρ denotes the fluid density, u is the velocity vector, p represents pressure, μ is the dynamic viscosity, T is the temperature, c_p is the specific heat at constant pressure, k denotes thermal conductivity, Q is the internal heat source term, and f represents body forces.

The CFD simulation procedure for wind load analysis is illustrated in Fig. 3, with the numerical computations carried out in Fluent.

(a) Geometry modeling: The geometric model of the jacket platform's topside modules is created. During modeling, key shape features that affect wind load calculations should be preserved,

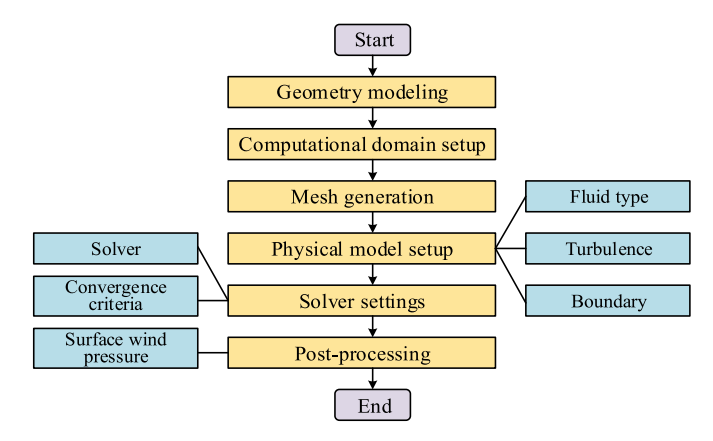


Fig. 3. CFD simulation procedure for wind load.

while minor structural details can be omitted to reduce mesh complexity and ensure successful mesh generation.

- (b) Computational domain setup: A sufficiently large computational domain is established to prevent the simulation results from being influenced by boundary conditions.
- (c) Mesh generation.
- (d) Physical model setup: The fluid is defined as incompressible air, and the turbulence model selected is the $k-\omega$ model. Boundary conditions are specified as follows: the inlet is set as a velocity-inlet, the outlet as a pressure-outlet, the top and bottom boundaries as no-slip walls, and the lateral boundaries as symmetry. At the velocity inlet, a user-defined function (UDF) is implemented based on the atmospheric boundary layer wind speed profile. A power-law distribution is adopted to describe the variation of wind speed with height(Sindi et al., 2025), as expressed in Eq. (6).

$$V(z) = V_{ref} \left(\frac{z}{z_{ref}}\right)^{\alpha} \tag{6}$$

where, z denotes the height above the ground, V(z) is the wind speed at height z, V_{ref} is the wind speed at the reference height z_{ref} , and α is the power-law exponent, which characterizes the surface roughness.

- (e) Solver settings: The SIMPLE algorithm is selected, with the convergence residual set to 0.001.
- (f) Post-processing: The main focus is on extracting the total wind load
- (3) Surrogate model construction

A surrogate model is constructed using the Kriging method to fit and calculate wind loads. Surrogate models are commonly used to represent complex physical systems mathematically and can be regarded as transfer functions that provide output results for given inputs. The Kriging model does not require the formulation of specific polynomial terms or mathematical expressions, making it more convenient to use. Additionally, it includes an error correction term, which further enhances the correlation between model variables and thereby improves accuracy. The Kriging model assumes that the true relationship between the system response and the input variables can be expressed as shown in Eq. (7).

$$y(x) = \sum_{i=1}^{n} \beta_i f_i(x) + z(x)$$
(7)

where, y(x) represents the approximation function, n is the number of sample points, $f_i(x)$ is a linear or nonlinear function of x, β_i is the estimated regression coefficient, and z(x) is a random function with a mean of zero.

The prediction process of the Kriging model can be expressed as shown in Eq. (8).

$$\begin{cases} \widehat{y}(x^*) = f(x^*)\widehat{\beta} + r(x^*)^T \gamma \\ \gamma = R^{-1}(y - f\widehat{\beta}) \end{cases}$$
(8)

where, r is the correlation vector between the prediction point and the sample points, R is the correlation function, and $\hat{\beta}$ is the estimate of β , which can be expressed as shown in Eq. (9).

$$\widehat{\beta} = \frac{f^T R^{-1} \mathbf{y}}{f^T R^{-1} f} \tag{9}$$

(4) Wind load prediction

The Kriging model is fitted to the sample points to determine the values of the correlation parameters in the model. Using the trained model, by inputting different values of the independent variables, the

model can automatically calculate the wind load under specific wind direction and speed conditions. This enables rapid computation of wind loads.

2.1.2. Wave load

The calculation of wave loads on the jacket platform can generally be divided into four steps, as illustrated in Fig. 4.

- (1) Determination of sea state parameters. The sea state parameters to be determined mainly include two categories: wave parameters and ocean environment parameters. Wave parameters primarily consist of wave height, period, and wavelength, which describe the characteristics of the waves. Ocean environment parameters mainly refer to water depth.
- (2) Selection of wave theory. To calculate the wave loads on a jacket platform, an appropriate wave theory should be selected based on the actual sea conditions. Broadly, wave theories can be classified according to the wave pattern into deterministic and random wave theories.

Based on the degree of linearization, they can be divided into linear and nonlinear wave theories. The Airy wave theory is a typical linear wave theory, which assumes that the nonlinear effects induced by the free surface motion of waves can be neglected, thereby ignoring the nonlinear characteristics of waves. Linear wave theory is suitable when the wave height is relatively small. However, in practical engineering, the wave steepness, defined as the ratio of wave height to wavelength, is not infinitesimally small but relatively large. In extreme sea conditions, such as storms, high-order nonlinear effects of waves become significant. Nonlinear wave theories provide predictions of wave shape, velocity fields, and wave forces that are closer to actual sea conditions and are suitable for scenarios with high waves and strong nonlinear effects. The choice of wave theory should be flexibly made according to the actual sea environment. In general, deep-water waves can be calculated using linear wave theory and Stokes wave theory, while shallow-water waves are mainly calculated using cnoidal wave theory. In practical engineering, the wave height H, wave period T, and water depth d are usually known parameters. Based on the dispersion relationship, the wavelength L can be determined. The applicable range of simplified wave theories is therefore as follows(Othman and Mohd, 2024; Tatum et al., 2016).

- 1) When $d/L \geq 0.2$ and $H/d \leq 0.2$, linear wave theory is adopted.
- 2) When $d/L \ge 0.1$ and H/d > 0.2, Stokes theory is adopted.
- 3) When d/L < 0.1, cnoidal wave theory is adopted.

In practical applications, the wavelength can be calculated from ocean environmental parameters using the dispersion relationship. A suitable wave theory is then selected based on the established criteria.

The above study on periodic and deterministic wave theories provides a foundation for analyzing real random sea states. Periodic waves constitute the fundamental components of random waves. Such representative waves offer a clear benchmark for studying real random sea conditions and can be applied to load analysis under a single typical sea state or for extreme condition simulations. To describe real random sea states, wave spectra are often employed. A wave spectrum is a statistical tool that characterizes the distribution of wave energy over frequency or wavenumber and serves as the basis for simulating random waves. Unlike a single periodic wave, real ocean waves are inherently random processes, with their heights, periods, and phases varying randomly in space and time. Wave spectra allow the statistical properties of waves to be quantified, thereby reflecting real random sea scenarios. Commonly used representative wave spectra include the Pierson-Moskowitz spectrum, and the JONSWAP spectrum. The construction of wave spectra from actual monitoring data generally involves the following steps.

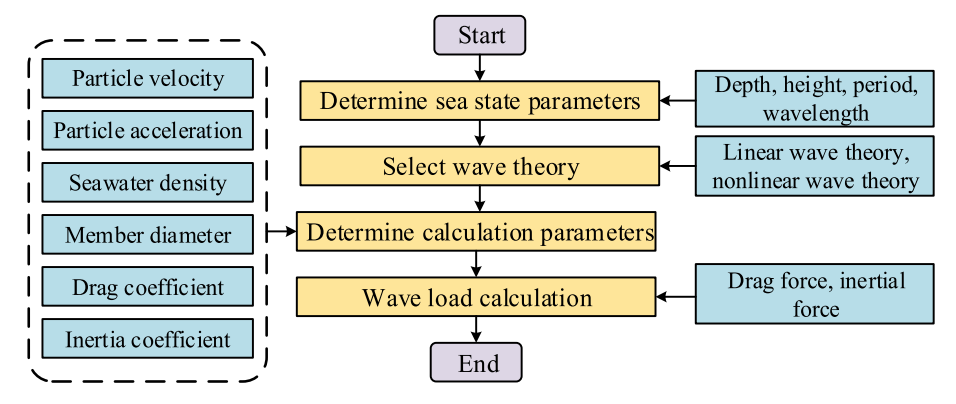


Fig. 4. Wave load calculation procedure.

- 1) Data acquisition: Obtain measured time series of wave heights or wave spectra data.
- Fourier analysis: Transform the time-domain wave height signal into the frequency domain to determine the energy distribution across different frequency components.
- 3) Spectrum smoothing and fitting: Smooth the discrete spectrum based on the measurement data to obtain the significant wave height, peak period, and spectral shape parameters. Under certain conditions, the spectrum can be fitted into a standard wave spectrum form.
- 4) Frequency discretization and random phase assignment: Discretize the continuous spectrum into several frequency components, determine the amplitude of each component according to the spectral density, and assign a random phase to each component to generate a random time-domain wave sequence.

Using this approach, historical observation data can be transformed into random wave inputs that reflect both statistical characteristics and time-domain fluctuations, providing a foundation for simulating realistic environmental conditions.

- (3) Determine calculation parameters. Once the sea conditions and wave theory have been established, the velocity and acceleration of water particles at different positions can be determined. In addition, to further calculate wave loads, key parameters such as seawater density, member diameter, drag coefficient, and inertia coefficient should be specified. When marine biofouling occurs on the aged jacket platform, the corresponding load amplification factor should also be taken into account.
- (4) Wave load calculation. The jacket structure is composed of slender cylindrical steel pipes. The wave loads acting on the members can be calculated using the Morison equation, which sums the drag force and the inertia force (Shehata et al., 2022). The wave load on spatial members is expressed in vector form as shown in Eq (10).

$$\overrightarrow{f} = f_x \overrightarrow{i} + f_y \overrightarrow{j} + f_z \overrightarrow{k} = \frac{1}{2} C_d \rho A \overrightarrow{U}_n \left| \overrightarrow{U}_n \right| + C_m \rho V_0 \overrightarrow{U}_n$$
(10)

where, \overrightarrow{U}_n represents the velocity perpendicular to the axis of the platform member, $\dot{\overrightarrow{U}}_n$ denotes the acceleration perpendicular to the member, A is the projected area per unit height in the wave direction, V_0 is the displaced volume per unit height, C_d is the drag coefficient, and C_m is the inertia coefficient.

The unit vector along the member axis and its projections in the three directions can be expressed as in Eqs (11) and (12).

$$\overrightarrow{e} = e_x \overrightarrow{i} + e_y \overrightarrow{j} + e_z \overrightarrow{k} \tag{11}$$

$$\begin{cases} e_x = \sin \alpha \cos \beta \\ e_y = \sin \alpha \sin \beta \\ e_z = \cos \beta \end{cases}$$
 (12)

The water particle velocity vector along the axis of the member, \overrightarrow{u} , is given in Eq. (13). The total velocity vector \overrightarrow{U}_n can then be expressed as shown in Eq. (14).

$$\overrightarrow{u} = u_x \overrightarrow{i} + u_y \overrightarrow{j} + u_z \overrightarrow{k} \tag{13}$$

$$\overrightarrow{U}_n = U_x \overrightarrow{i} + U_y \overrightarrow{j} + U_z \overrightarrow{k} = \overrightarrow{e} \times \overrightarrow{u} \times \overrightarrow{e}$$
(14)

From Eqs (13) and (14), the following expression can be derived.

$$\begin{cases} U_x = u_x (1 - e_x^2) - u_z e_x e_z \\ U_y = u_x e_x e_y - u_z e_z e_y \\ U_z = u_z (1 - e_z^2) - u_x e_x e_z \end{cases}$$
(15)

Accordingly, the wave load components per unit length on the jacket members can be obtained, as shown in Eq. (16).

Based on the expression for the distribution of wave loads along the members, combined with the velocity and acceleration formulas of water particles, the wave load acting on any structural member can be calculated.

2.1.3. Current load

The current-induced load on the jacket platform can also be calculated using the Morison equation. In engineering practice, ocean currents are typically considered as steady flows, allowing the inertia term to be neglected while retaining only the drag force component. The calculation formula for current-induced load is given in Eq. (17) (Zhang et al., 2020).

$$f_c = \frac{1}{2} C_d \rho A U_c^2 \tag{17}$$

where, f_c represents the current-induced load per unit length on the structure, A is the projected area of the structural member per unit length facing the flow, and U_c is the current velocity.

When calculating current-induced loads, it is first necessary to obtain the current velocity profile—i.e., the flow velocities at various depths—based on measured data. To compute the total current force, a method similar to that used for wave load calculation can be applied: discretize the structure, calculate the drag force on each element, and then sum the contributions to obtain the total current-induced force. When both wave and current are present simultaneously, the drag force

should be calculated based on the combined horizontal velocity resulting from the superposition of current velocity and wave particle velocity.

2.2. Jacket platform modeling

Jacket platform modeling consists of two main parts: the construction of the global finite element model of the intact jacket platform, and the modeling of aging-related defects. First, a global finite element model of the intact platform is developed. Different element types are selected based on the characteristics of various structural components, with appropriate boundary conditions applied and material properties assigned. Subsequently, aging-related defects such as corrosion, fatigue cracks, and mechanical dents are introduced into the intact model to complete the modeling of the aged jacket platform. In modeling the aged structure, a multi-scale modeling approach is adopted. At locations where local defects occur, fine-scale elements are used to capture the detailed features, while the global jacket structure is modeled using larger-scale elements. Coupling between different element types is achieved by defining appropriate connections at their interfaces. This strategy ensures modeling accuracy while significantly reducing the total number of elements, thereby improving computational efficiency.

2.2.1. Modeling of the entire structure

The finite element modeling of the overall jacket platform structure can be carried out following the procedure illustrated in Fig. 5.

- (1) Define structural components. The structural components of the jacket platform to be modeled and analyzed can be divided into two main parts: the topside module and the foundation structure. The topside module includes the deck, deck beams, upper support structures, and various equipment and facilities related to production and living. The foundation structure consists of the jacket and piles, which form the primary focus of the analysis.
- (2) Element type selection. Select appropriate element types for modeling each structural component of the jacket platform. The element types commonly used in jacket platform modeling include beam elements, pipe elements, solid elements, shell elements, spring elements, and mass elements. The selection should be based on the geometry and load-bearing characteristics of each structural component. The specific element types available for use are listed in Table 1.
- (3) Set geometric properties. Define the geometric attributes of the elements based on the structural parameters of each module of the jacket platform.
- (4) Set material properties. The jacket structure and pile foundation can be defined using an elastoplastic material model, while other components such as the topside module can be modeled with a

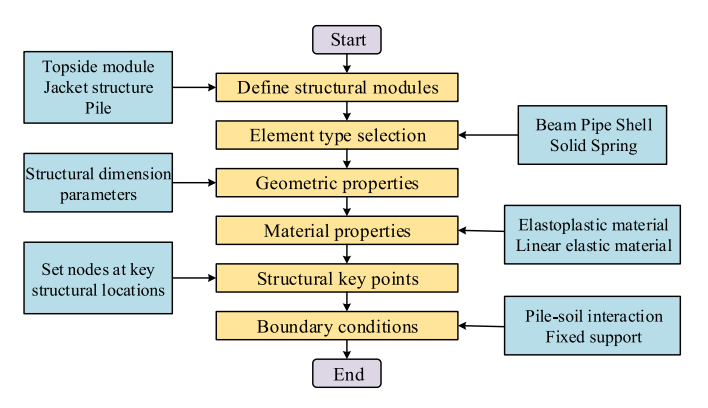


Fig. 5. Overall finite element model of the jacket platform.

- linear elastic material. It is also necessary to specify key parameters such as density, elastic modulus, Poisson's ratio, yield strength, and tangent modulus.
- (5) Define key structural points. During modeling, intersection points of members, locations of concentrated loads, points of abrupt change in cross-sectional properties, and the connection points between piles and the design mudline should be defined as nodes, serving as key points for structural analysis.
- (6) Set boundary conditions. When considering the nonlinear interaction between pile and soil and when geotechnical data are available, nonlinear spring elements should be applied to the piles of the jacket platform to simulate pile–soil interaction. The embedded portion of the piles should be discretely modeled based on soil properties. At each pile element node, horizontal springs should be defined using p–y curves to simulate lateral resistance, and vertical springs should be defined using t–z curves to represent shaft friction. At the pile tip, vertical springs based on q–z curves should be used to simulate end bearing resistance (El-Din and Kim, 2014). Under certain conditions, the boundary conditions can also be simplified as fixed supports to reduce computational complexity. (Karimi et al., 2025; Yang et al., 2017).

2.2.2. Modeling of structural defects

As jacket platforms progress into their mid-to-late operational stages, various forms of structural degradation induced by ageing begin to emerge. These structural defects can significantly reduce the platform's ultimate strength and compromise its load-bearing capacity. Accurate simulation of these defects is a critical step in evaluating the residual ultimate strength of the structure. In this study, three typical types of structural defects—corrosion, fatigue cracks, and mechanical dents—are selected as case studies. Their respective modeling approaches are analyzed and discussed, along with their impacts on the structural ultimate bearing capacity.

The dimensions of a jacket platform generally range from tens to hundreds of meters. However, defects such as pitting corrosion, fatigue cracks, and mechanical dents typically occur at localized areas. Especially for pitting and cracks, their sizes are often on the order of centimeters or millimeters. Relative to the entire jacket platform, these are considered minor and localized damages. When modeling an aged jacket platform, using beam elements to create a global macroscopic model can significantly reduce computational effort but struggles to capture the microscopic mechanisms of local structural damage. Conversely, constructing a detailed model entirely with shell or solid elements can better represent microscopic defects but drastically increases computational cost and may cause convergence issues, making it impractical for engineering applications. This study introduces the concept of multi-scale finite element analysis: embedding fine-scale models locally within the global macroscopic model to describe local structural defects. This approach ensures computational accuracy while reducing the computational burden, thereby addressing this challenge effectively.

(1) Multiscale FEA model

The overall concept of multi-scale finite element modeling is to solve local subproblems to construct basis functions that reflect the microscopic characteristics of the material. These small-scale details are then incorporated into the larger-scale domain, where the finite element method assembles the global stiffness matrix on a coarse mesh, enabling accurate and efficient solutions at the macroscopic scale.

The establishment of the multi-scale finite element model for the jacket platform can be carried out in the following five steps.

(a) Establish the macroscopic model. Use macroscopic large-scale elements such as beam and pipe elements to model the main

- structure of the jacket platform, omitting small-scale details and retaining only the overall geometric characteristics.
- (b) Identify critical local regions. Determine the local areas that require refinement based on factors such as stress concentration, component importance, and the extent of structural damage.
- (c) Establish the microscopic model. Use high-precision Solid or Shell elements to perform detailed modeling of the local regions.
- (d) Establish the connection relationship. Establishing a reasonable connection between the macroscopic and microscopic scale elements is a key step. In this study, the Multi-Point Constraint (MPC) method is adopted to realize the coupling between different scale elements. The MPC method is based on the principle of degree-of-freedom coupling and constraint equations, where the degrees of freedom of the microscopic model nodes are linked to certain nodes of the macroscopic model through constraint relations, ensuring consistency in key degrees of freedom behavior between the two models. The mathematical expression is shown as follows.

$$u_m = T \cdot u_M \tag{18}$$

where, u_m denotes the degrees of freedom at the microscopic node connection, u_M denotes the degrees of freedom at the macroscopic node connection, and T is the transformation matrix.

The MPC method enables compatibility of degrees of freedom between different types of elements without the need for transitional meshing. It preserves the geometric continuity of the structure and also supports large displacement scenarios.

(2) Structural defects

In the defect modeling of aging jacket platform structures, the effects of age-related defects such as corrosion, fatigue cracking, and mechanical denting on the structural performance are taken into account. Details are shown in Fig. 6.

(a) Corrosion

Corrosion can be classified into two types: uniform corrosion and pitting corrosion. Uniform corrosion can be modeled by idealized wall thickness reduction, which can be implemented by directly modifying the cross-sectional dimensions of beam elements, without the need for a multiscale finite element model. Since different elevations of a jacket platform are exposed to varying marine environments, their corrosion behavior and characteristics differ accordingly. Based on the nature and rate of corrosion as well as the surrounding marine conditions, the jacket platform can be divided into five corrosion zones: the atmospheric zone, splash zone, tidal zone, fully submerged zone, and mud zone (Jia et al., 2025). A schematic of these zones is shown in Fig. 7.

The atmospheric zone refers to the area above sea level that does not come into contact with seawater but is exposed to humid sea winds. The corrosion in this zone is relatively mild compared to other regions, with a typical corrosion rate of 0.03–0.08 mm/a. The splash zone is located above the mean high tide line and is regularly wetted by splashing seawater. With ample supply of both seawater and oxygen, it is the most severely corroded region on the jacket platform, with a corrosion rate of 0.3–0.5 mm/a. The tidal zone lies between the mean high tide and mean

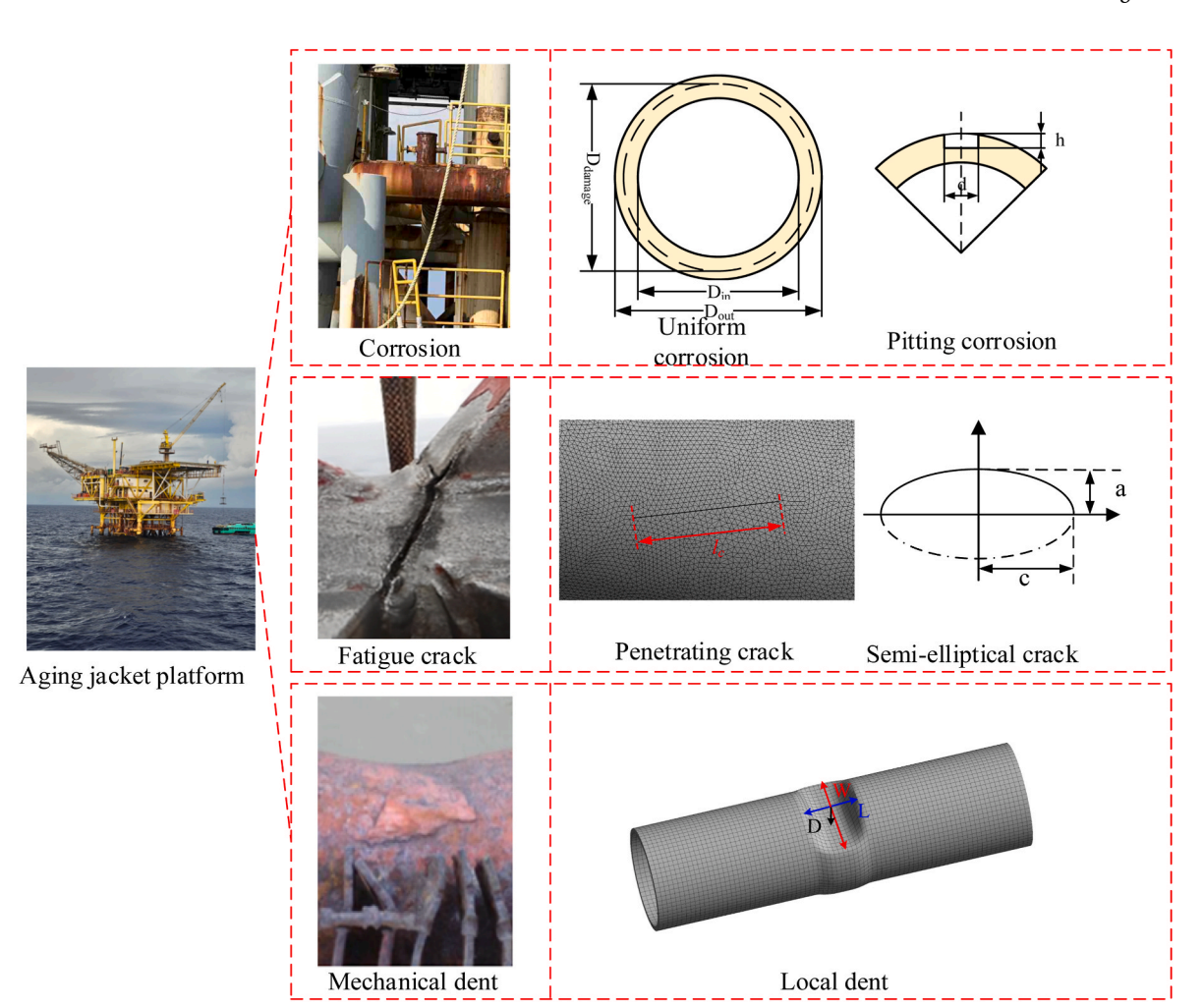


Fig. 6. Modeling of structural defects in aging jacket platforms.

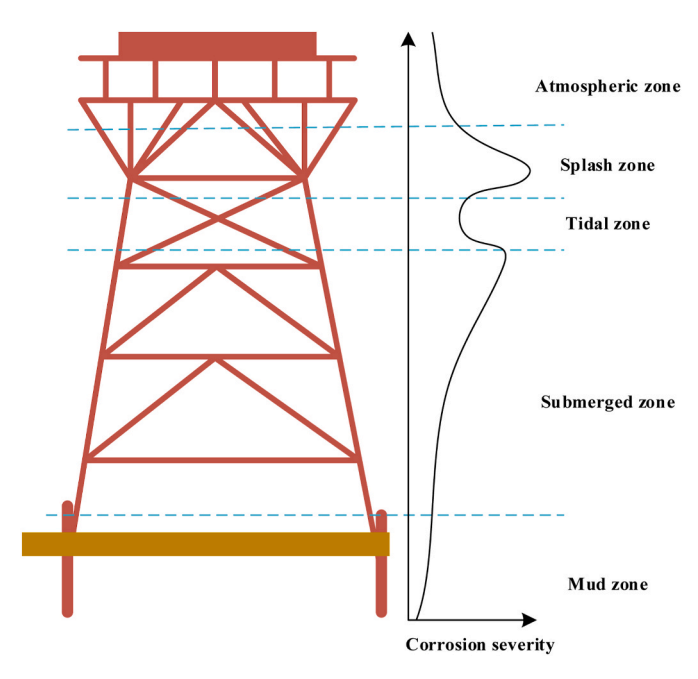


Fig. 7. Corrosion zone division.

low tide lines, where oxygen-rich seawater comes into periodic contact with the steel surface, causing corrosion. This region typically experiences the second-highest level of corrosion after the splash zone, with a rate of 0.1–0.37 mm/a. The fully submerged zone is located below the mean low tide line and is not exposed to the atmosphere. Corrosion in this region is mainly influenced by factors such as dissolved oxygen, temperature, and salinity. In general, corrosion in deep-water areas is relatively mild, with rates ranging from 0.13 to 0.25 mm/a. The seabed zone refers to the buried portion of the pile legs. Due to extremely low oxygen content, the degree of corrosion in this region is minimal.

Pitting corrosion is a form of localized corrosion that requires the introduction of a multi-scale local refined model for accurate representation. The surface of a pit is typically circular in shape (Yang et al., 2021). The geometry of a pitting pit can generally be modeled as cylindrical, conical, or ellipsoidal. As long as the severity of corrosion is similar, variations in the pit shape generally do not have a significant impact on the calculated ultimate strength. In this study, cylindrical pits are used for modeling. A pit can be characterized by two parameters: the pit diameter d and pit depth d. Typically, the pit diameter for ships and offshore structures ranges from 25 mm to 80 mm. The corrosion severity of a specific section of a jacket platform component can be described using two parameters: the Degree of Pitting (DOP) and the Degree of Volume Loss (DOV).

$$DOP = \frac{1}{A} \sum_{i=1}^{n} \frac{\pi d_i^2}{4}$$
 (19)

$$DOV = \frac{1}{At} \sum_{i=1}^{n} (A_{pi} \times h_i)$$
 (20)

where, A represents the surface area of the component, d_i is the diameter of the ith pit, t is the thickness of the component, and h_i is the depth of the ith pit.

(b) Fatigue crack

Under cyclic loads such as wind and waves, areas with stress concentrations such as welds are subjected to long-term alternating stresses, which can easily lead to crack initiation and propagation. In tubular joints of the jacket structure, where welding is concentrated, local stress concentrations are more severe, making these areas particularly prone to fatigue cracks. The crown point, toe, and heel of tubular joints are all common fatigue hotspots. Based on the location of the cracks within the component, they can be classified as through-thickness cracks, surface cracks, and embedded cracks. This study focuses on the effects of through-thickness cracks and surface cracks at tubular joints on the overall structural performance.

Through-thickness cracks are cracks that extend across the entire thickness of a structural component. Typically, cracks that propagate through more than half the thickness are considered through-thickness cracks, and they have the most significant weakening effect on the structural load-bearing capacity. Modeling of through-thickness cracks can be carried out using solid or shell elements. During modeling, two approaches can be employed to simulate through-thickness cracks. One approach involves using modeling techniques such as Boolean operations to create a narrow discontinuous region, thereby simulating severe cracking (Ji et al., 2016). The other approach directly separates the nodes on either side of the crack to release the constraints on their degrees of freedom.

The length and position of the crack are the two key parameters used to describe through-thickness cracks. This study considers the scenario in which cracks propagate circumferentially along the weld or around the branch pipe at tubular joints. Since branch pipes vary in size, the length of their intersection curves with the main pipe also differs. To provide a unified measure of crack propagation at different locations, a relative crack length is defined to quantify the degree of crack propagation, as shown in Eq. (21).

$$\lambda = \frac{l_c}{l_c} \tag{21}$$

where, λ denotes the relative crack length, l_c is the actual crack length, and l_w is the length of the intersection curve of the brace with the chord.

Surface cracks are located on the surface of structural components, with depths relatively small compared to the component thickness. In modeling, surface cracks are typically simplified as semi-elliptical cracks. A semi-elliptical crack is a representative three-dimensional surface crack geometry, whose profile in a cross-section perpendicular to the surface forms a semi-ellipse. The key geometric parameters used to describe a semi-elliptical crack are the minor semi-axis a and the major semi-axis a. Here, a represents the depth of the crack perpendicular to the surface, while a lies along the surface direction; a is the total crack length on the surface. The ratio a characterizes the sharpness of the crack tip—generally, the sharper the crack, the faster it propagates. In modeling, solid elements are required to accurately simulate semi-elliptical cracks.

(c) Mechanical dent

The dent defect on a jacket platform refers to the localized plastic deformation that occurs on the surface of steel tubular members due to external mechanical actions, such as lifting impacts, collisions with ships or underwater structures, or dropped-object impacts. These actions result in a depressed or indented area. Typically, the affected region is relatively small and confined to the vicinity of a single cross-section. Therefore, mechanical dents are considered local defects and require a multi-scale finite element model for accurate representation, using solid or shell elements for simulation. Due to the highly random nature of dent formation, the geometric shapes of dents can vary significantly. During modeling, actual measurements from the field are necessary, and a dent model should be constructed based on the observed geometry and parameters. Mesh refinement is required in the region where the dent is located.

The location, geometric parameters, and orientation of a mechanical dent are the three key factors influencing its impact. Due to the randomness of collision events, mechanical dents may occur at various positions such as the main leg, diagonal braces, or horizontal braces, each affecting the overall structural ultimate strength to different extents. The geometric parameters of a dent mainly include its length, width, and depth, which describe the affected area and the severity of the damage. In addition, the orientation of the dent opening also influences the ultimate strength of the structure. Even for dents of identical size, differing orientations can lead to varying effects on the structural capacity (Punurai et al., 2020).

2.3. Ultimate load capacity calculation

The next step is to calculate the ultimate strength of the jacket platform Pushover analysis, also known as nonlinear pushover analysis, is based on the principle of elastoplastic structural analysis and is an effective method for evaluating the overall collapse resistance and ultimate bearing capacity of a structure. Additionally, pushover analysis can examine the failure process and failure modes of the structure under loads exceeding the design values. The procedural flow of pushover analysis is shown in Fig. 8.

- (1) Apply the design environmental loads. The loading process can be divided into two load steps. In the first load step, gravity and buoyancy loads are applied to the structure. The gravity load should account for both the self-weight of the jacket platform and the weight of the upper modules on the platform. These gravity and buoyancy loads should remain constant throughout the subsequent analysis. In the second load step, the design environmental load parameters are used to apply the three lateral loads of wind, waves, and current. These three lateral loads, considering the most unfavorable direction for the structure, should be applied simultaneously in the same direction.
- (2) The loads are gradually increased. The lateral environmental loads are incrementally amplified to perform the pushover analysis. During the pushover process, it is necessary to consider the P-Delta effect caused by the weight of the upper modules when the structure undergoes plastic deformation and large displacement of the platform.

- (3) Monitor the structural response. During the pushover analysis, the overall structural response, as well as the yielding and failure mechanisms of components, can be monitored and tracked.
- (4) Determine whether the ultimate state has been reached. The assessment of whether the jacket platform has reached its ultimate state can be made using a combination of methods. As the jacket is a statically indeterminate structure, when members yield or nodes fail, internal forces redistribute within the remaining members and nodes of the structural system. When the remaining structural system, or a part of it, forms a mechanism the overall stiffness matrix of the structural system becomes singular. As shown in Eq. (22), this condition indicates that the structure has reached its ultimate state. Additionally, when the pushover curve becomes flat, and a slight increase in load causes a significant displacement increase or a descending branch appears, this is also considered a sign of structural collapse and attainment of ultimate load-bearing capacity.

$$\det(K) = 0 \tag{22}$$

- (5) Plotting the result curve. When the structure reaches its ultimate load-bearing capacity, the pushover curve can be plotted to reflect the pushover process of the structure. The pushover curve records the entire progression of the structure from linear elastic response, to elastoplastic response, and finally collapse. Initially, when the applied environmental load is less than the yield load *Fy* of the members, the structure responds linearly elastically, and the corresponding pushover curve is a straight or nearly straight line passing through the origin. When the load exceeds *Fy*, the members begin to yield successively, and the curve's slope gradually approaches zero. However, the platform does not collapse immediately but continues until the ultimate load *Fu* is reached. When the load exceeds *Fu*, the platform enters the collapse stage.
- (6) Evaluation of results and interpretation. When the jacket platform reaches its ultimate state, that is, at the peak point of the pushover curve, the base shear force of the jacket platform or the environmental load is taken as the measure of the ultimate

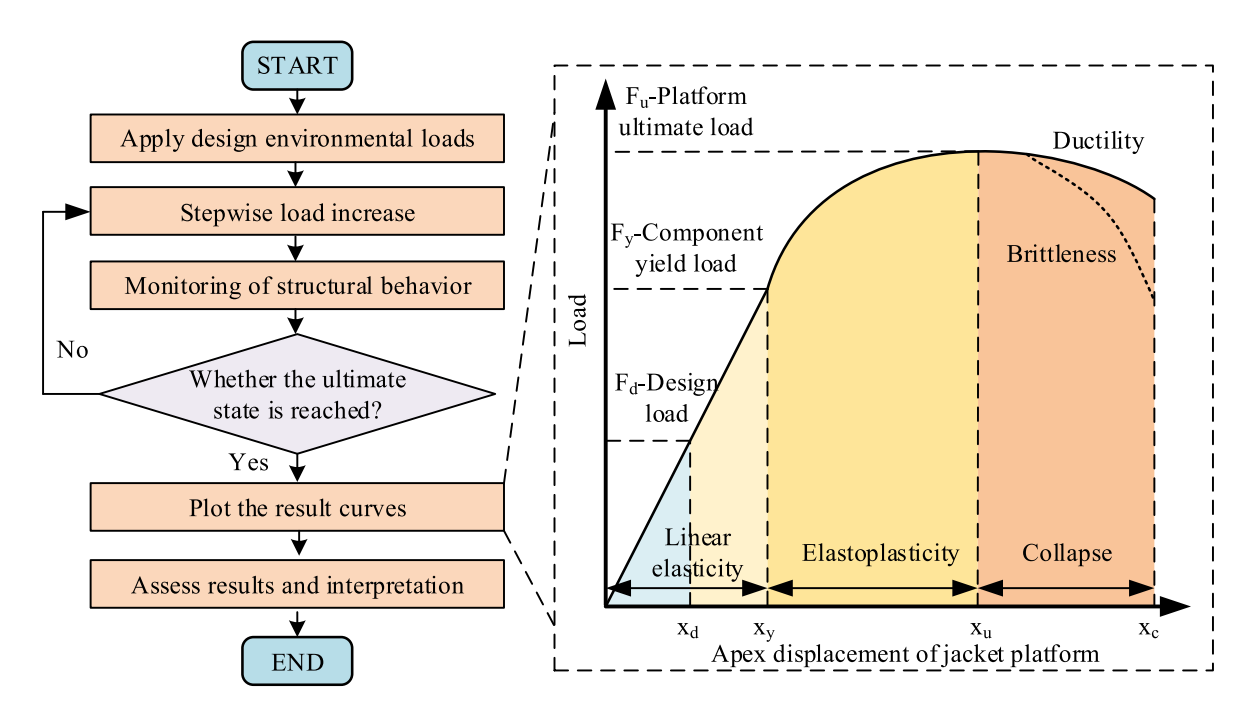


Fig. 8. Pushover analysis procedure for jacket platforms.

bearing capacity. In addition, the Reserve Strength Ratio (RSR) is also a key indicator for assessing the load-bearing capacity of the jacket platform. The RSR reflects the resistance level of the platform structural system and holds significant importance in overall performance design and evaluation. The definition of RSR is given by Eq. (23).

$$RSR = \frac{F_u}{F_d} \tag{23}$$

where, F_u represents the environmental load or base shear force corresponding to the platform's collapse, and F_d denotes the design environmental load or the base shear force of the platform under the design environmental load.

2.4. Digital twin-driven health monitoring

The above steps enable the calculation of environmental loads and the residual ultimate strength of the structure. Within the DHE framework, based on these calculation processes, digital-twin-driven real-time structural health monitoring can be realized. In Module 1 of the DHE, advanced measurement technologies such as buoys and radar can be used to measure parameters including wind speed, wind direction, wave height, wave period, and ocean current velocity profiles in near real time. Furthermore, the detection and identification of structural defects are also critical steps. Due to the harsh marine environment and the concealed nature of defects, some aging defects can be difficult to detect. The reliability of ultimate strength calculations fundamentally depends on the accuracy of defect identification. Overall, methods for defect detection and identification can be classified into three main categories: remote unmanned inspection, manual periodic inspection, and hybrid approaches combining the two. This study recommends the hybrid approach, whereby sensor-equipped systems are used for remote monitoring of damage-critical areas and locations difficult for manual access, while manual inspections using appropriate equipment are conducted periodically to detect structural defects. This enables timely measurement and updating of defect parameters. In terms of specific defect detection techniques, visual inspection, ultrasonic and radiographic testing, magnetic particle testing, and structural health monitoring have been widely applied. Common defect identification methods are summarized in Table 2. In practice, the selection of methods should be flexible, based on the sensitivity and characteristics of each technique.

Then, these parameters are transmitted to the analysis center via Module 2. At the analysis center, the methods proposed in this study are applied to compute and update environmental loads and residual ultimate strength, as illustrated in Fig. 9.

In practice, environmental parameters change continuously. By combining surrogate models with analytical methods, near real-time calculation of environmental loads can be achieved. In contrast, changes in defect parameters are relatively slow and exhibit higher randomness. Using the proposed methods, various defects can be efficiently modeled and analyzed, allowing timely updates of the residual ultimate strength. Based on the relationship between these two in-

Table 1 Element type.

Element type	Specific element options	Application
Pipe	PIPE16, PIPE59, PIPE288	Jacket structure, Pile
Beam	BEAM4, BEAM188	Jacket structure, Pile,
		Deck beam
Shell	SHELL43, SHELL63, SHELL91,	Deck
	SHELL181	
Solid	SOLID45, SOLID95, SOLID46, SOLID	Equipment and facilities
	186, SOLID191	
Spring	COMBIN39, COMBIN40	Pile-soil interaction

Table 2 Structural defect detection and identification methods(Sindi et al., 2024).

Method	Type of damage		Remark	
	Corrosion	Crack	Denting	
Visual examination, close-up tool-aided examination	✓	1	1	Small equipment items are required, such as a hammer, flashlight, calipers, and measuring tape.
Digital imaging	✓	1	1	Automatic processing is usually required.
Leak or pressure testing	1	1		Detects pit corrosion and small cracks.
Dye-penetrant testing, chemical sensor examination		/		Affected by cleanliness.
Ultrasonic testing Magnetic particle detection	✓	1		Time consuming. Applicable only for magnetic materials; detects only (sub) surface defects
Strain gauge-based assessment	✓	1		Detects reductions in stiffness caused by damage
Electromagnetic field examination		1		Detects surface and subsurface cracks at weld seams
X-radiometry		1		Requires specialized operator expertise.
Acoustic emission or natural frequency testing	1	/		Used for preliminary assessments; performed by specialized companies.
Thermal imaging	1	1		Applicable to a limited range of situations
Moiré contouring			✓	Reveals deformation patterns of dents; an emerging technique

dicators, the overall safety margin of the jacket platform can be defined, as expressed in Eq. (24).

$$\eta = \frac{C}{D} > \eta_{cr} \tag{24}$$

where, C represents the residual ultimate strength, D denotes the environmental load, and η_{cr} is the critical value of the safety index.

The safety index of the jacket platform fluctuates with changes in environmental loads and residual ultimate strength. Consequently, it can provide a real-time reflection of the platform's safety condition and guide on-site decision-making, thereby realizing digital twin–driven health monitoring.

In practice, environmental parameters change continuously. This study combines surrogate models with analytical methods to analyze environmental parameters within a few seconds, enabling rapid calculation and timely updating of environmental loads. In contrast, structural defect parameters change relatively slowly. They are generally updated through periodic inspections. Using the proposed method, each inspection record of defect parameters can be efficiently modeled and analyzed, typically completing nonlinear finite element analysis within tens of minutes, thereby enabling updates of residual ultimate strength. Compared with traditional CFD and ultimate strength calculation methods, the proposed approach reduces computation time from the scale of hours to seconds or minutes. This greatly improves computational efficiency, meets engineering application requirements, and supports rapid decision-making under extreme conditions.

In practical engineering, by integrating Modules 1 and 2 of the DHE framework to establish a system for measuring and transmitting health parameters, and combining it with the computational method proposed in this study for the digital twin model, updates and calculations of environmental loads and residual ultimate strength can be performed.

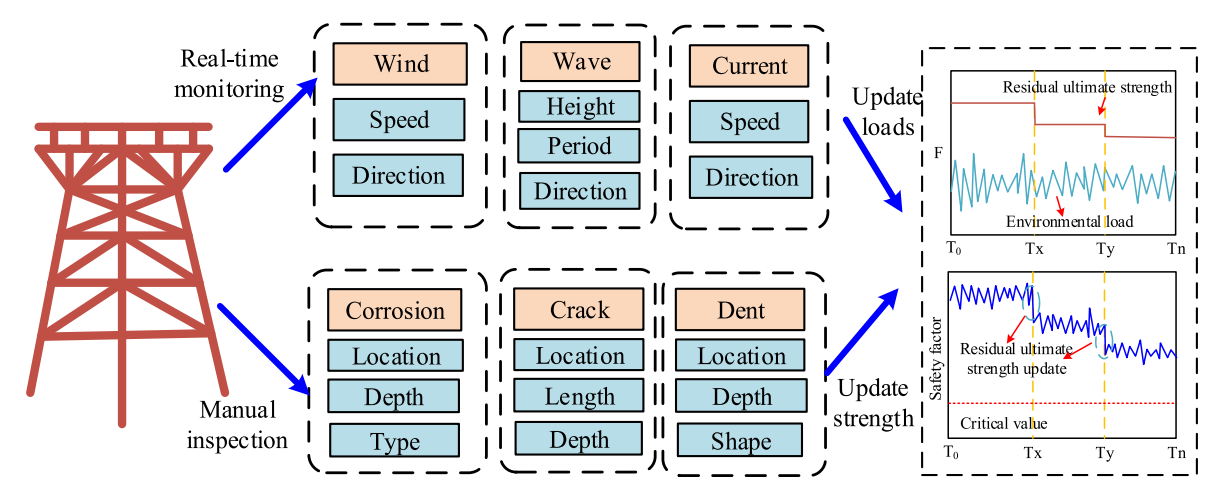


Fig. 9. Real-time on-site data analysis.

This, in turn, reflects the structural safety margin, supports further structural response analysis, and feeds the results back to the field to aid decision-making. In this way, a complete digital twin–driven health monitoring system for aging jacket platforms can be realized.

3. Case study

In the method proposed in this work, the calculation of environmental loads and residual ultimate strength are the two key steps, and are also crucial for realizing the digital twin. Therefore, the calculation methods for environmental loads and residual ultimate strength are verified to demonstrate the effectiveness of the approach.

The jacket platform is shown in Fig. 10. The platform is designed for a water depth of 100 m. The topside consists of four levels,

accommodating various facilities and equipment related to production and living needs. The four main legs are arranged in a double-inclined symmetrical configuration, and the bracings adopt an X-shaped layout. In the modeling process, Beam elements are used to model the lower jacket structure, the inter-level bracing structure of the deck, and the deck beams. The deck itself is modeled using Shell elements, while the equipment and facilities placed on the deck are modeled using Solid elements. Regarding materials, a nonlinear material model is assigned to the jacket structure. In this study, the material is assumed to be conventional structural steel, without considering the strengthening effect of Z-direction performance steel in critical welded joints and thick plates. A bilinear kinematic hardening ideal elastoplastic model is adopted, with a yield strength of 360 MPa and a tangent modulus of 763 MPa. The topside structure is modeled using a linear elastic material.

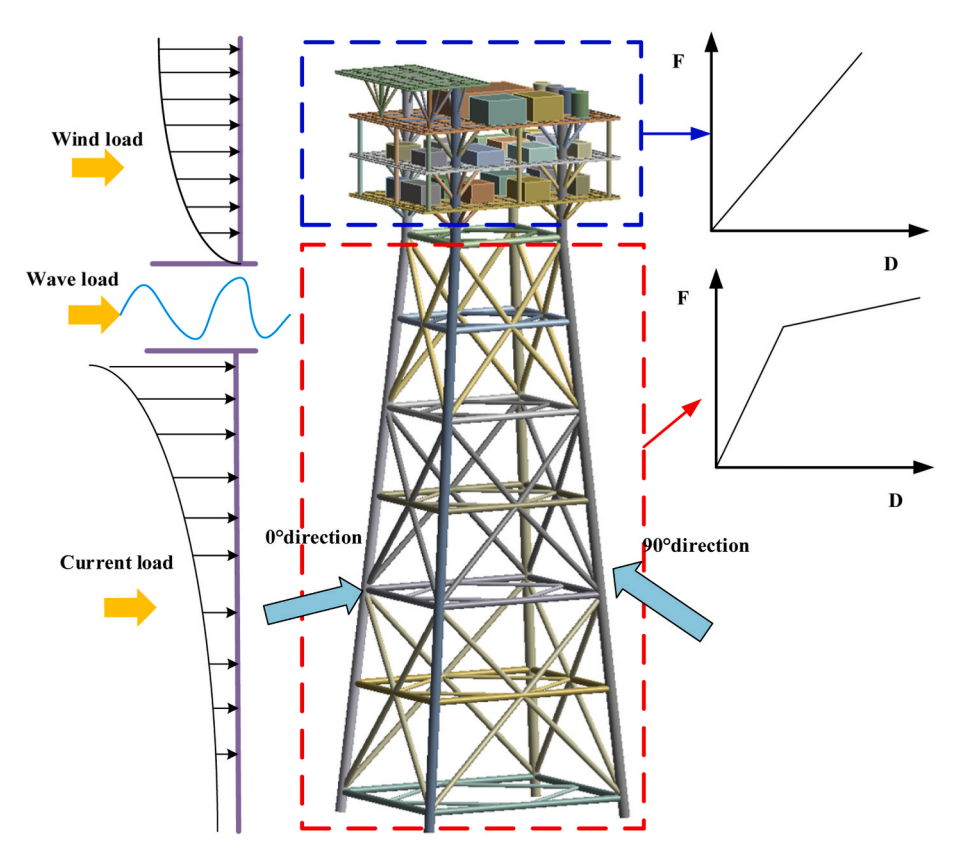


Fig. 10. Offshore jacket platform.

3.1. Environmental load calculation results

Due to the structural symmetry of the jacket platform, the environmental load calculation is carried out within the range of 0° – 90° . The wind speed is set to range from 0 to 60 m/s. First, sample points are obtained using the sampling method, after which a CFD model is established to compute the actual wind loads at different sample points. The generated data points are then used to train the Kriging model.

When training the surrogate model, this study employed the Latin Hypercube Sampling (LHS) method to generate sample points. A CFD calculation is required for each sample point, which introduces a considerable computational cost. The use of LHS ensures a more uniform sample distribution, preventing clustering in certain regions and making the sample space more representative. This approach helps improve analysis efficiency and reduces the computational burden of engineering simulations. In the actual calculations, sample sizes of 20, 30, 40, and 50 were considered. Additionally, 10 sample points were randomly selected as a validation set to assess the computational accuracy of the model. The model accuracy for different sample sizes is compared in Fig. 11.

As shown in Fig. 11, with the increasing number of samples, the error gradually decreases, indicating that the model accuracy improves continuously. At the same time, the coefficient of determination R^2 increases, demonstrating an enhanced level of model fitting. When the sample size reaches 50, the average error is only 1.36 %, the maximum error is 4.82 %, and the R^2 value is approximately 1, indicating that the model has achieved high accuracy and meets the application requirements. Furthermore, observing the trend of error reduction, the improvement in model accuracy becomes limited as the sample size increases. Meanwhile, the computational time grows rapidly with more samples. Considering both accuracy and computational cost, a sample size of 50 was adopted for the current validation. In practical engineering applications, the sample size can be further increased to enhance model accuracy.

When the sample size is 50, the CFD model results and the Kriging model outputs for the validation set are shown in Fig. 12. The results indicate that both computational methods exhibit consistent trends in wind load variation, demonstrating that the surrogate model can effectively capture changes in wind speed and direction and subsequently compute the corresponding wind loads. Furthermore, the wind load predictions are very close, with the maximum error occurring at a wind speed of 23.41 m/s and a wind direction of 3.42°, but even this maximum error is only 4.82 %. This indicates that the surrogate model has achieved high predictive accuracy and demonstrates good fitting performance.

The primary objective of this section is to calculate the overall wind

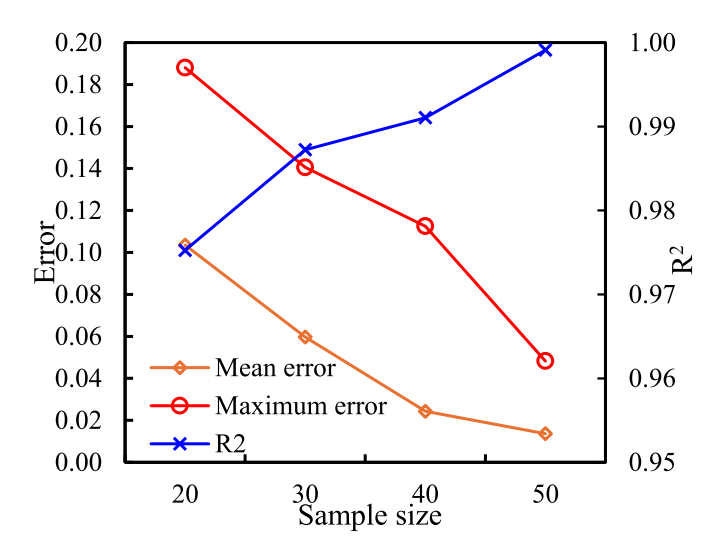


Fig. 11. Comparison of model accuracy.

load magnitude. In practical engineering, the overall wind load can be computed using time series of measured wind speed and wind direction. The proposed surrogate modeling approach allows for rapid updating of wind load values under varying wind speeds and directions, capturing the dominant wind load magnitudes while avoiding unnecessary model complexity. The calculation range can cover all directions as well as wind speed ranges under both normal and extreme conditions. In addition, the CFD model accounts for turbulence effects and aerodynamic interference, yielding results that more closely reflect actual conditions.

The characteristic parameters of the extreme marine environment are a wave height of 20.34 m, a wave period of 12.63 s, and a current velocity of 2.23 m/s. Combined with the water depth data, the wavelength can be calculated to be approximately 246 m by solving the dispersion relation. Referring to the criteria for wave theory selection in Section 2.1.2, the ratio of water depth to wavelength d/L is approximately 0.4065, and the ratio of wave height to water depth H/d is 0.2034, indicating that Stokes wave theory should be applied. Based on the Morison equation, the combined wave-current load is calculated.

Four typical directions—0°, diagonal, 45°, and 90°—were selected for wave-current load calculations. For each direction, two representative conditions were considered: waves and currents in the same direction, and waves and currents in opposite directions, in order to further analyze the influence of wave and current propagation directions on the load calculation results. Figs. 13 and 14 show the fluctuations of the combined wave-current loads over one period for the same and opposite directions, respectively. When the wave and current directions are the same, the maximum combined wave-current load occurs at the 90° direction, reaching 2.52×10^{7} N, while the minimum occurs at the 0° direction, with a value of 2.17 \times 10^{7} N. When the wave and current directions are opposite, the maximum load still occurs at the 90° direction, reaching 1.53×10^7 N, and the minimum occurs at the 0° direction, at 1.32×10^7 N. The maximum load is significantly smaller in the opposite case due to the vector difference of water particle velocities. In addition, both the load fluctuations and the directions of maximum values exhibit noticeable differences. Therefore, in engineering applications, the influence of wave and current directions on load calculations must be considered.

Furthermore, to validate the effectiveness of the proposed wave load calculation method under real random sea conditions, calculations were performed using random wave spectra. The sea state was characterized using statistical wave parameters, and the Pierson–Moskowitz spectrum was employed to simulate the waves. Two sea state conditions were considered: a normal condition represented by a significant wave height of 4.61 m and a peak period of 5.36 s, and an extreme condition represented by a significant wave height of 20.34 m and a peak period of 12.63 s. Wave loads were calculated in the 0° and 90° directions, with the results shown in Fig. 15. The figure illustrates that wave loads exhibit random fluctuations, and the peak wave forces under extreme conditions are significantly higher than those under normal conditions. This further demonstrates that the proposed load calculation framework is applicable for computations under real random sea-state conditions.

To further validate the effectiveness of the environmental load calculation method, the parameters of wind, wave, and current were adjusted by varying the environmental return periods. Taking the 90° direction of the jacket platform as an example, calculations were performed under different environmental load conditions. The parameters of the environmental loads are listed in Table 3. Fig. 16 presents the computed maximum values of wind load, as well as combined wave and current loads. As the return period of the loads increased, wind speed, wave height, period, and current velocity all gradually increased, and the resulting wind and wave—current loads exhibited a corresponding upward trend. Overall, the wave—current loads are significantly greater than the wind loads, indicating that they constitute the primary environmental loads acting on the jacket platform. The proposed calculation method can rapidly respond to changes in environmental load

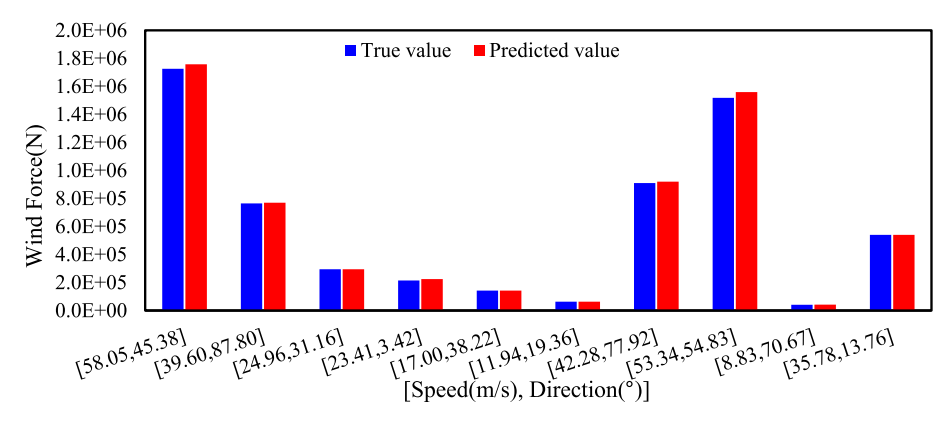
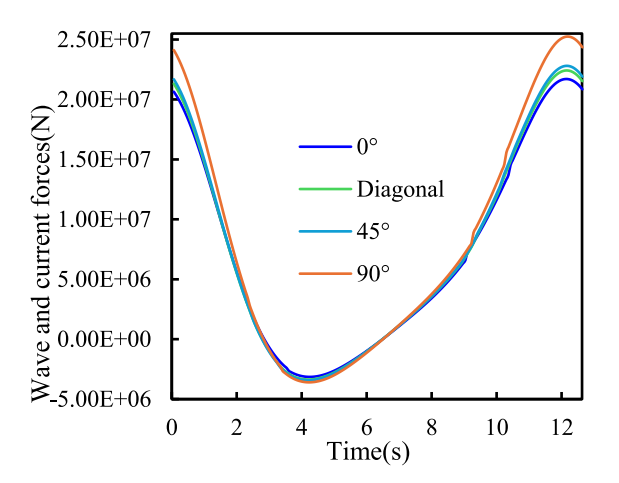


Fig. 12. Wind load calculation results.



 $\textbf{Fig. 13.} \ \ \textbf{Wave-current force in co-directional condition.}$

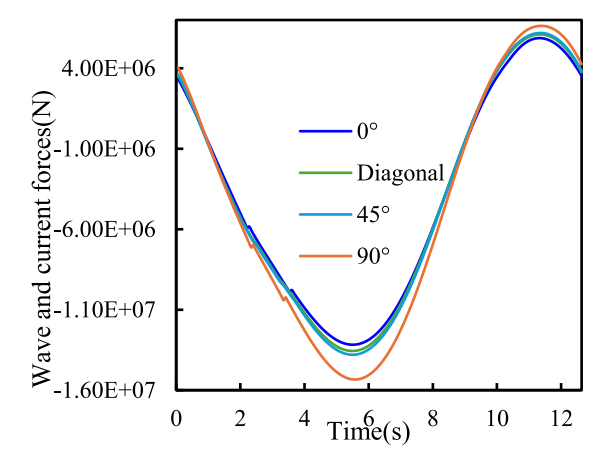


Fig. 14. Wave-current force in counter-directional condition.

parameters and efficiently compute the corresponding environmental loads.

3.2. Ultimate strength calculation of the intact jacket platform

First, the ultimate strength of the intact jacket platform is calculated. Based on the design environmental load, a step-by-step magnification is applied to perform pushover analysis on the platform.

The load-bearing capacity curve of the jacket platform is shown in Fig. 17, and the calculated results of its ultimate strength are presented in Fig. 18. As shown, the ultimate strength of the platform exhibits a

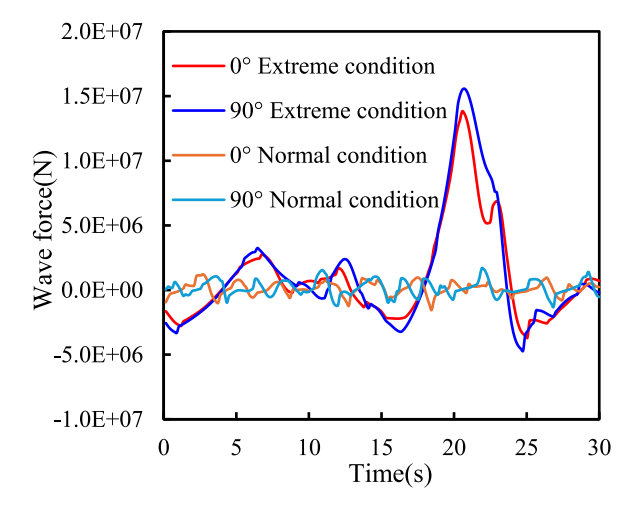


Fig. 15. Wave forces under random sea states.

Table 3 Environmental load parameters.

Load ID	Wind speed(m/s)	Wave height (m)	Period (s)	Current velocity(m/s)
1	18.42	4.61	5.36	0.48
2	32.71	16.18	11.36	1.58
3	37.46	20.34	12.63	2.22
4	40.93	23.43	13.49	2.76
5	43.77	25.98	14.16	3.23
6	46.22	28.20	14.72	3.67
7	48.40	30.18	15.20	4.08
8	50.37	31.99	15.62	4.46
9	52.18	33.65	16.01	4.83
10	53.86	35.21	16.36	5.18

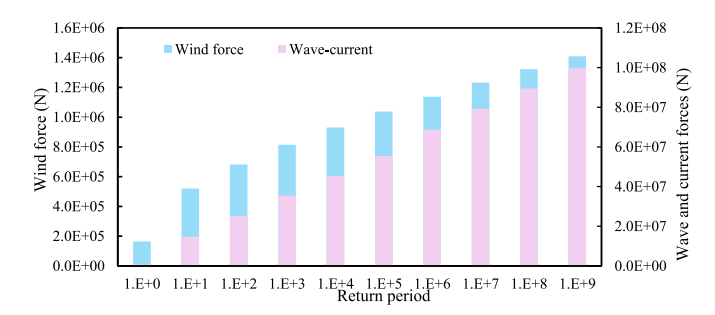


Fig. 16. Results of environmental load calculations.

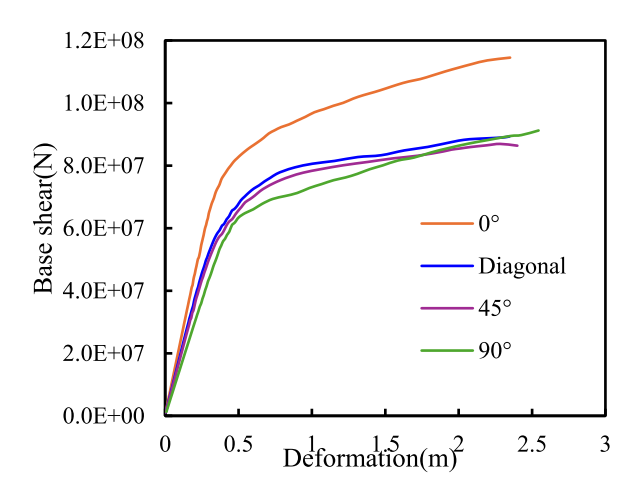


Fig. 17. Ultimate load capacity curve of the intact platform.

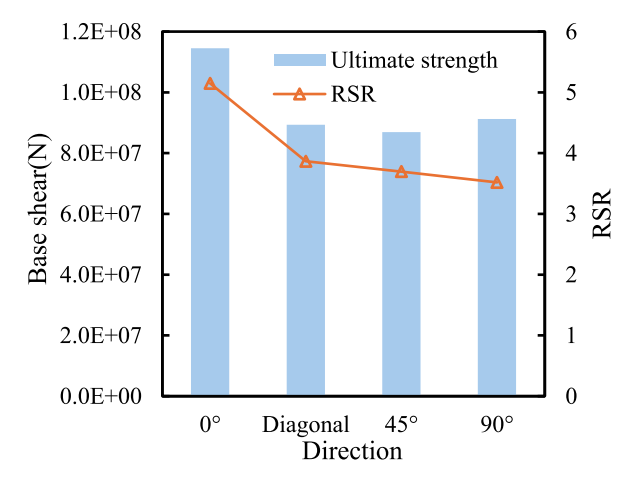


Fig. 18. Ultimate strength of the intact platform.

trend of initially decreasing and then increasing from the 0° to the 90° direction. The lowest ultimate strength occurs in the 45° direction, at 8.69×10^{7} N, while the highest is in the 0° direction, approximately

 1.15×10^8 N. However, the RSR shows a steadily decreasing trend, dropping from 5.15 in the 0° direction to 3.52 in the 90° direction. Although the ultimate strength is relatively high in the 90° direction, the platform also experiences greater environmental loading in that direction, resulting in the lowest RSR value—indicating that this remains the most vulnerable direction for the platform. Overall, the collapse mechanisms in all four directions demonstrate ductile behavior, indicating that the structure possesses a degree of redundancy.

Stress contour plots at a moment before collapse in the 0° , 45° , and 90° directions are extracted, as shown in Fig. 19. From the figure, it can be seen that the maximum equivalent stress in the jacket platform exceeds the yield strength of the material in all three cases. The main legs of the platform serve as its primary load-bearing members, and significant stress concentrations are observed at their bases, where plastic deformation has already occurred. Additionally, considerable stress appears in the mid and lower diagonal braces, where preliminary plastic hinge mechanisms have formed. As the lateral loads continue to increase, these diagonal braces are likely to fail, which would lead to overloading of the main legs and eventually result in the collapse of the jacket platform.

To verify the effectiveness of the multi-scale finite element modeling approach proposed in this study, locally refined models using solid and shell elements were introduced into selected parts of the intact platform, as shown in Fig. 20. Subsequently, pushover analyses were conducted on the jacket platform from the 0° and 90° directions, respectively.

The load capacity curves of the multi-scale finite element models are shown in Fig. 21. A comparison of the ultimate load capacity results obtained from different finite element models is presented in Fig. 22. As shown in the figures, the load capacity curves of the beam-solid and beam-shell models exhibit the same trend, and the overall variation pattern is consistent with the results in Fig. 17. The ultimate load capacity values computed using the multi-scale finite element models are also similar to those from the single-scale models, with the ultimate capacity in the 0° direction being significantly higher than that in the 90° direction. In terms of numerical results, there are varying degrees of deviation between the multi-scale models and the beam-only model. The largest deviation occurs in the beam-shell model under the 0° loading condition, but even in this case, the deviation is only 0.3 %. A comparison of the number of nodes and elements for different finite element models is also shown in Fig. 23.

To further illustrate the advantages of the multiscale finite element

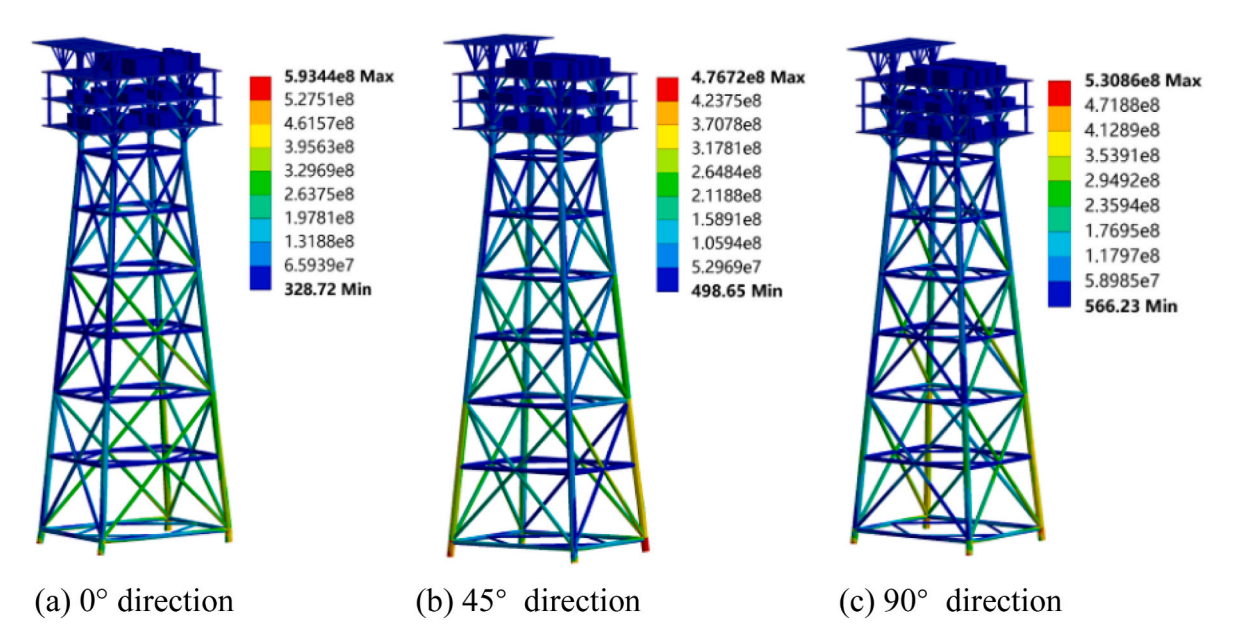


Fig. 19. Stress contours in different directions.

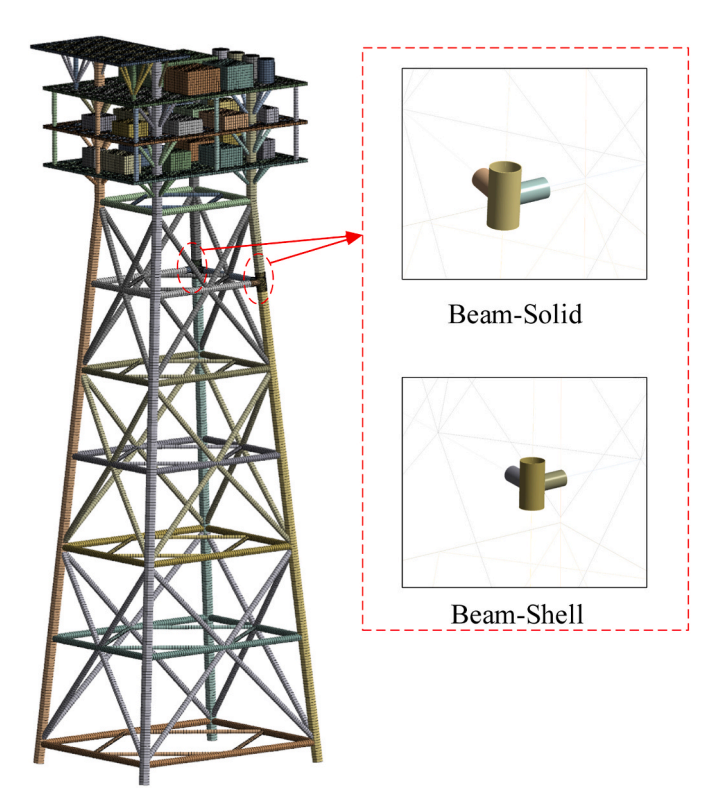


Fig. 20. Multiscale finite element model of the intact platform.

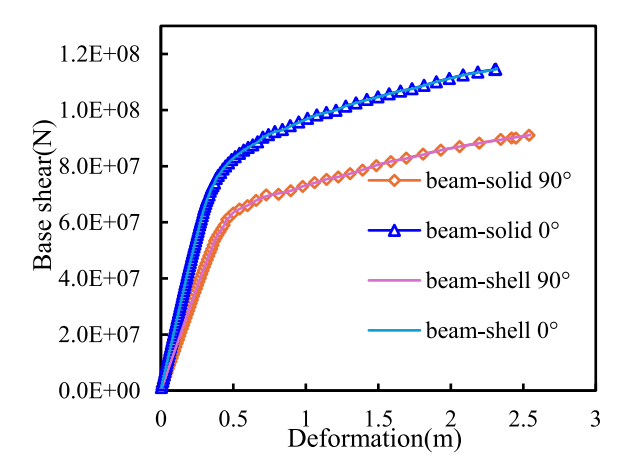


Fig. 21. Load-bearing capacity curve of the multiscale model.

model, jacket platform models were established using single-scale beam elements, beam-shell elements, beam-solid elements, shell elements, and solid elements. The different modeling approaches were compared in terms of the number of nodes, number of elements, computation time, and calculated ultimate strength, with the results shown in Table 4. The results indicate that models constructed entirely with shell or solid elements have the highest number of nodes and elements and require the longest computation time, significantly exceeding those of beam elements and multiscale elements. Moreover, due to the large mesh size, these models exhibit slow iteration, convergence difficulties, and substantial computational resource consumption. Although fine models built with solid or shell elements generally yield the highest accuracy, the enormous computational cost makes them impractical for engineering applications and, in some cases, even unsolvable. In contrast, among the other three modeling approaches, the beam model has the fewest nodes and elements, indicating the highest computational

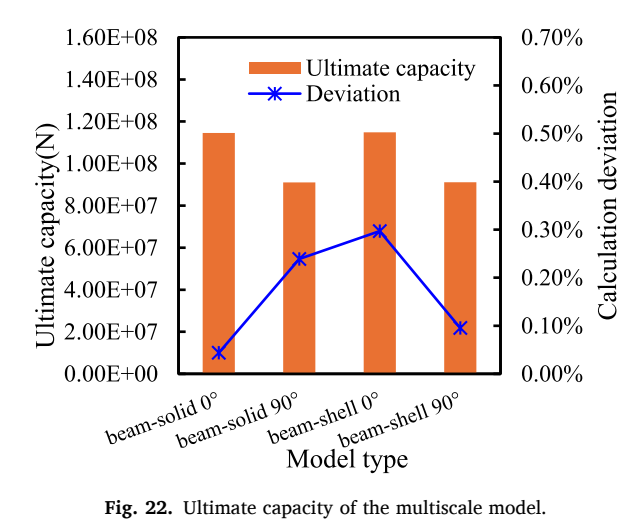


Fig. 22. Ultimate capacity of the multiscale model.

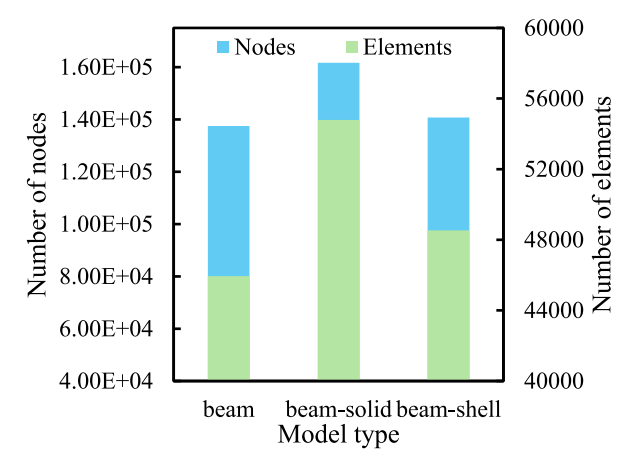


Fig. 23. Comparison of the number of nodes and elements in the model.

Comparison of different modeling approaches.

	Beam	Beam- solid	Beam- shell	Solid	Shell
Number of nodes	137474	161685	140746	4764129	300971
Number of elements	45941	54790	48532	1736132	223021
Computation time (h)	0.5	0.65	0.6	23	8
Ultimate strength (0°, N)	1.145E8	1.146E8	1.148E8	1.023E8	1.035E8

efficiency, followed by the beam-shell and beam-solid models. Overall, although the introduction of local detailed models reduces computational efficiency, it does not cause a dramatic increase in the number of nodes and elements, and the computation remains within an acceptable range. At the same time, the calculated results from the three modeling approaches are comparable. The multiscale finite element model maintains computational accuracy while reducing computational cost, validating the effectiveness of the proposed modeling method. For practical modeling of local defects in aging jacket platforms, beam-solid or beam-shell elements should be reasonably selected based on the type and characteristics of structural defects, while also considering computational efficiency.

3.3. Residual ultimate strength assessment of aging jacket platforms

Based on the intact jacket platform described above, corrosion, cracks, and mechanical dent defects are introduced to investigate the effects of structural defects on the ultimate strength of the jacket platform, and to further validate the effectiveness of the modeling method proposed in this study.

It should be noted that the primary purpose of examining the residual ultimate strength of aging jacket platforms is to verify the effectiveness of the proposed multiscale finite element model, the defect modeling approach for aged structures, and the residual ultimate strength evaluation method. The defect parameters used in the calculations are prescribed values rather than actual field measurements. Furthermore, since pitting, fatigue cracks, and mechanical dents are localized defects, their dimensions are relatively small compared with the entire platform. In this study, some defect parameters were selected to represent extreme conditions, which allows a clearer observation of the reduction in the overall structural ultimate strength and facilitates the investigation of how residual ultimate strength varies with different defect parameters. In addition, under circumstances such as prolonged lack of maintenance or severe accidental impacts(Mujeeb-Ahmed and Paik, 2021), extreme structural defects such as penetrative corrosion(Alizadeh et al., 2024) and large-scale dents may indeed occur(Lin et al., 2022; Punurai et al., 2020). This makes it possible to investigate the structural response under the most unfavorable conditions and to assess the lower bound of safety margins, thereby providing valuable references for understanding structural failure modes and conducting safety evaluations of offshore platforms under ultimate limit states.

3.3.1. Corrosion

The effects of two types of corrosion, uniform corrosion and localized pitting corrosion, on the ultimate strength of the jacket platform were studied separately. First, uniform corrosion was investigated. The upper bound of the corrosion rates in each region was taken as the current corrosion rate. The jacket platform section from -2 m to +2 m was defined as the tidal zone with a corrosion rate of 0.37 mm/year; from +2 m to +10 m as the splash zone with a corrosion rate of 0.5 mm/year; above +10 m as the atmospheric zone with a corrosion rate of 0.08 mm/year; and below -2 m as the submerged zone with a corrosion rate of 0.25 mm/year. Uniform corrosion was simulated by reducing the wall thickness. Different degrees of corrosion defects were applied to the jacket platform for pushover analysis. The residual ultimate capacity curves of the jacket platform are shown in Fig. 24. The variation of residual ultimate capacity and RSR values is shown in Fig. 25.

As shown in the figure, with the progressive increase in corrosion severity of the jacket platform, the inflection point of the load-displacement curve gradually decreases, and the displacement at

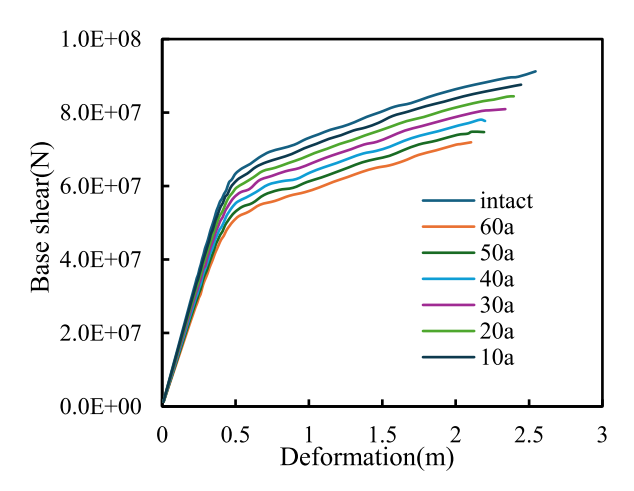


Fig. 24. Load-bearing capacity curve under uniform corrosion.

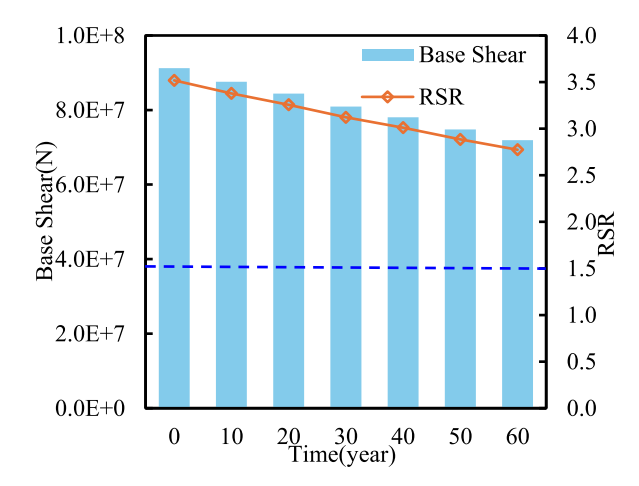


Fig. 25. Variation of load-bearing capacity under uniform corrosion.

ultimate capacity becomes smaller, indicating a reduction in platform ductility. In addition, the residual ultimate strength exhibits a steadily decreasing trend, roughly following a linear decline. The platform's ultimate strength decreases from an initial value of $9.12\times10^7~\rm N$ to $7.19\times10^7~\rm N$, and the RSR value drops from 3.52 to 2.77. Overall, uniform corrosion defects significantly affect a wide range of the jacket structure and result in a notable reduction in residual ultimate strength. The residual strength reserve threshold for this platform is 1.5. Based on the results shown in the figure, it can be concluded that the jacket platform still maintains a relatively high strength reserve.

Next, the influence of localized pitting corrosion on the ultimate bearing capacity of the jacket platform is further investigated. Based on the analysis results of the intact platform, it is evident that the lower region of the main legs experiences high stress and serves as a critical load-bearing area of the structure. This region is therefore defined as the damage-sensitive zone of the jacket platform. Using the beam-solid modeling approach, pitting corrosion defects are introduced in this area to better observe the resulting reduction in structural strength. The model is shown in Fig. 26.

Due to the inherent discrepancies in ultimate bearing capacity results between the multi-scale finite element model and the single beam-element model, a direct comparison may be affected. To intuitively evaluate the reduction in the structural strength of the jacket platform, the concept of the Residual Ultimate Strength Ratio (RUSR) is introduced. This metric is used to quantify the relative variation in the platform's remaining ultimate strength, as defined in Eq. (25).

$$RUSR = \frac{F_{RU}}{F_{II}} \tag{25}$$

where, F_U represents the ultimate bearing capacity of the intact multiscale model, while F_{RU} denotes the ultimate bearing capacity of the platform with defects.

It is assumed that the DOP values are 0.1, 0.15, and 0.2, respectively. For each DOP, the corrosion depth is taken as 0.5 times the wall thickness and as through-thickness (equal to the full wall thickness), resulting in a total of six experiments. The load-bearing capacity curves of the jacket platform under different pitting scenarios are shown in Fig. 27, and the corresponding RUSR values are presented in Fig. 28. The results indicate that with increasing pitting intensity and corrosion depth, the residual ultimate strength of the jacket platform shows a clear decreasing trend. When the corrosion depth is 0.5 times the wall thickness and the DOP is 10 %, 15 %, and 20 %, the ultimate strength drops to approximately 97.2 %, 93.4 %, and 90 % of that of the intact platform, respectively. In the case of fully penetrating pitting, the reduction in residual ultimate strength becomes more significant, decreasing to approximately 90.5 %, 85.5 %, and 79 % of the intact

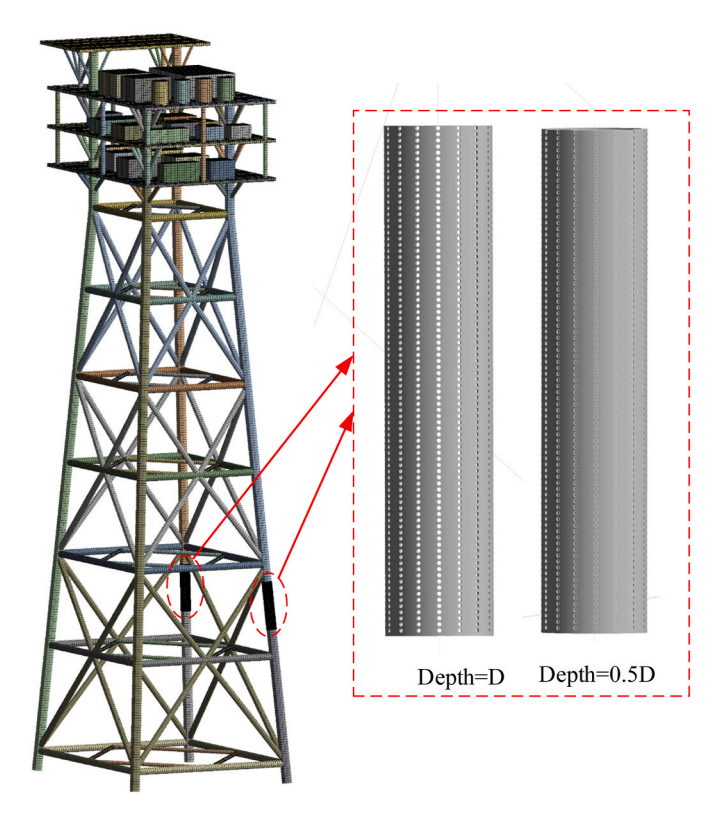


Fig. 26. Localized pitting defect model.

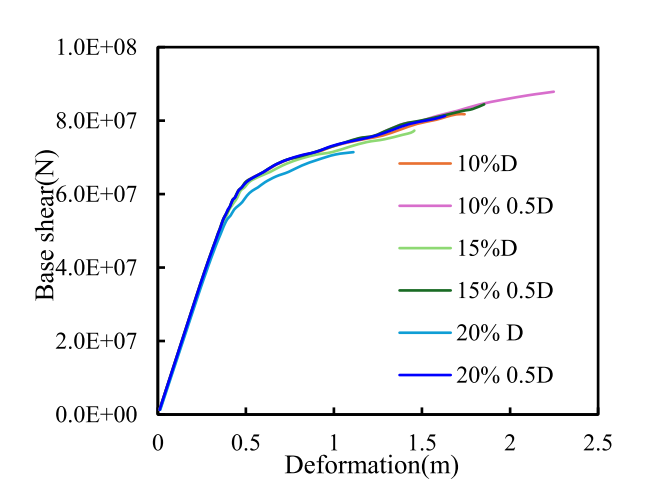


Fig. 27. Load-bearing capacity curve under pitting corrosion.

platform's strength under the same DOP values.

3.3.2. Fatigue crack

Fatigue cracks were introduced at the locations shown in Fig. 29 to investigate the influence of fatigue cracking on the ultimate strength of the jacket platform. First, through-thickness cracks were placed on the main legs of the platform at positions 1, 2, 3, and 4 along the tubular joints, by generating narrow slit openings. This setup was used to study the effect of through-thickness cracks on the load-bearing capacity of the jacket platform. It should be noted that, the analysis of through-thickness cracks on ultimate strength is conducted solely to verify the analysis and modeling methods proposed in the paper. In practical engineering, through-thickness cracks are unacceptable, as their occurrence indicates structural failure and requires immediate repair. Moreover, due to the implementation of regular inspections and maintenance, the likelihood of through-thickness cracks occurring is

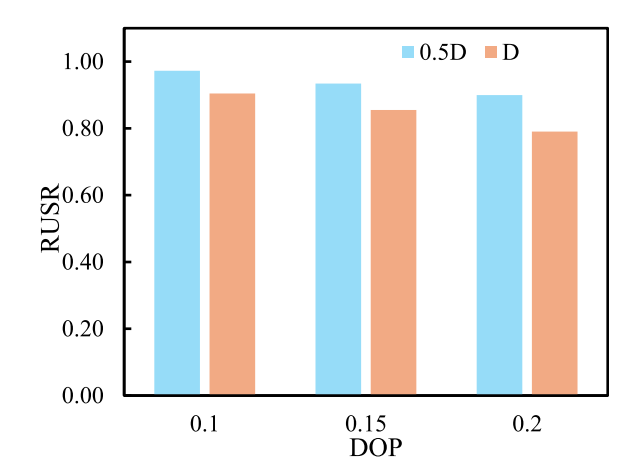


Fig. 28. RUSR calculation results under pitting corrosion.

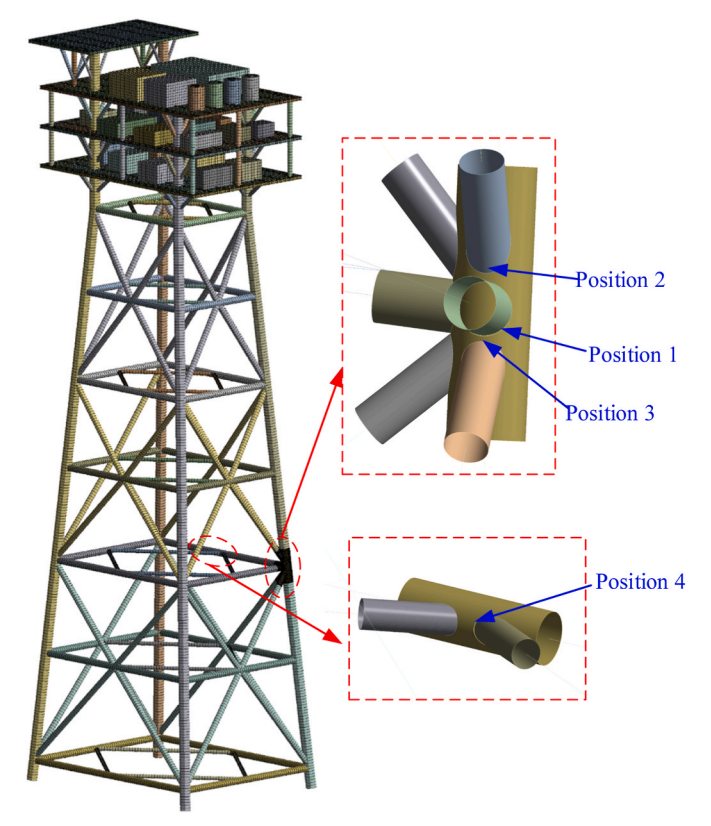


Fig. 29. Crack placement location.

relatively low. Through-thickness cracks represent the most severe crack propagation scenario. In the case studies, adopting through-thickness cracks allows for a more pronounced observation of strength reduction, facilitating the investigation of how different crack parameters influence the ultimate strength of the structure and thereby validating the effectiveness of the proposed modeling approach. Ji et al. (2016) and Wang et al. (2015) have considered through-thickness cracks in their studies on the ultimate strength of jacket platforms. This approach helps simplify the modeling process, determine the lower bound of safety margins, and yield more conservative assessment conclusions, while also supporting the study of failure modes under extreme damage conditions.

The beam–shell model was used for modeling, with the relative crack lengths assumed to be 0.1 and 0.2, respectively. The load-bearing capacity curves of the jacket platform are shown in Fig. 30, and the RUSR

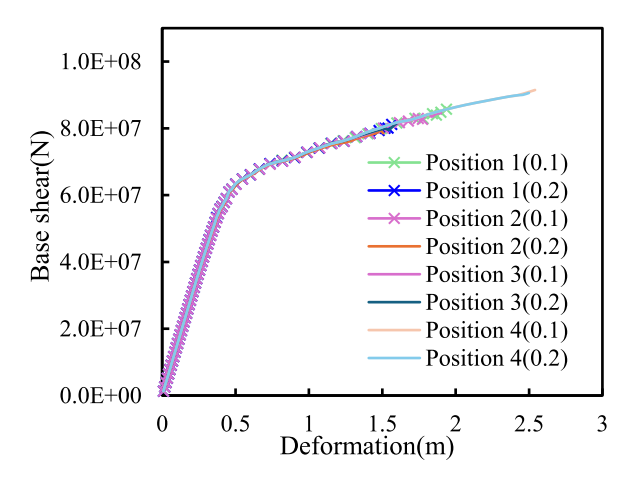


Fig. 30. Load-bearing capacity curve with penetrating crack.

results are presented in Fig. 31.

As shown in the figure, cracks at positions 1, 2, and 3 all result in a certain degree of reduction in the ultimate strength of the jacket platform, while the crack at position 4 has almost no effect. This is because positions 1, 2, and 3 are located on the main legs, which are key loadbearing components and damage-sensitive areas of the platform. Therefore, only cracks located in critical regions cause significant reductions in ultimate strength. When the relative crack length is 0.1, the cracks at positions 1, 2, and 3 reduce the ultimate strength of the jacket platform to 95.7 %, 92.6 %, and 94.3 % of the intact platform, respectively. When the relative crack length increases to 0.2, the cracks at positions 1, 2, and 3 cause more pronounced reductions in strength. This indicates that the more severe the crack propagation, the greater the structural impact. Among these, the crack at position 2 leads to a more significant strength reduction, with an RUSR of 88.5 %. The cracks at positions 1 and 3 have similar impacts on the structure. Overall, the crack at position 2 causes the most notable reduction in the ultimate strength of the jacket platform and represents a more critical location.

At the intersection of the brace and the main leg at position 1, a crack is simulated by disconnecting mesh nodes to study the effect of connection failure between the brace and the main leg on the ultimate strength of the structure. The ultimate load-bearing capacity curve of the jacket platform is shown in Fig. 32, and the calculated RUSR values are presented in Fig. 33. In the analysis, the relative crack lengths are assumed to be 0.2, 0.5, and 1, respectively. A relative crack length of 1 indicates complete disconnection between the brace and the main leg. Additionally, for the case of a relative crack length of 0.5, two scenarios are simulated: the crack appears in the upper region and in the lower region, respectively, to investigate the influence of crack location on the

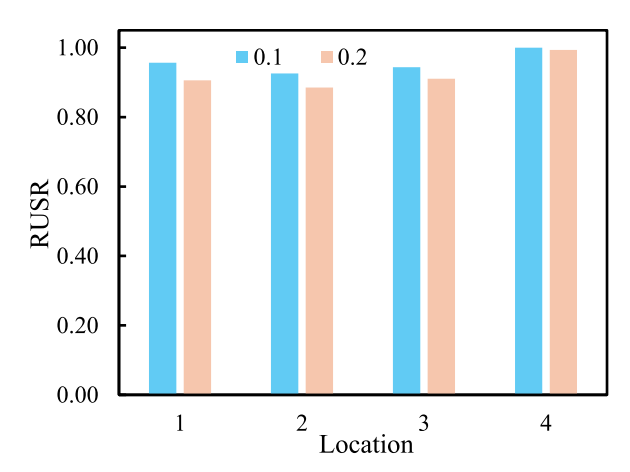


Fig. 31. RUSR calculation results under penetrating crack.

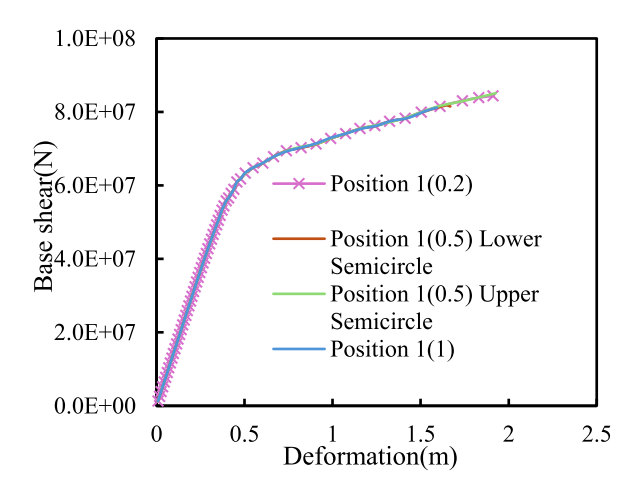


Fig. 32. Load-bearing capacity curve with node disconnection.

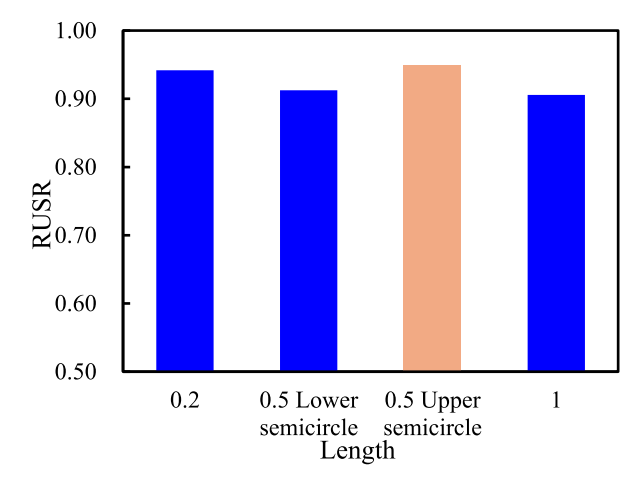


Fig. 33. RUSR calculation results under node disconnection.

results. When the crack is located in the lower region, the RUSR values for the three lengths are 94.2 %, 91.2 %, and 90.6 %, respectively. This indicates that as the crack length increases, the degree of damage at the brace-to-leg connection deepens, leading to a gradual decline in ultimate strength. When the brace is completely disconnected from the main leg, the platform's ultimate strength drops by approximately 9.4 %. Furthermore, for the case of a relative crack length of 0.5, placing the crack in the upper region of the brace-to-leg joint shows that cracks in the lower region result in a more significant reduction in ultimate strength under the same crack length. This demonstrates that even when the crack length is identical, its location has a varying impact on the structural capacity. Therefore, in practical engineering applications, both the crack length and its initiation location must be considered in a comprehensive assessment.

The beam-solid element modeling approach is used to introduce a surface semi-elliptical crack at the intersection region of the tubular joint at position 1. The major axes of the semi-elliptical cracks are assumed to be 0.005 m, 0.01 m, and 0.015 m, respectively, while the minor axes are assumed to be 0.05 m, 0.1 m, and 0.15 m, respectively. The reduction in the ultimate strength of the jacket platform under the influence of these surface semi-elliptical cracks is calculated, and the results are shown in Fig. 34. From the figure, it can be seen that surface semi-elliptical cracks have a clear and consistent impact on the platform's ultimate strength. When the crack length is constant, greater crack depth leads to lower residual ultimate strength. Similarly, for a constant crack depth, increasing the crack length also results in reduced residual ultimate strength. Surface cracks are a more common form of

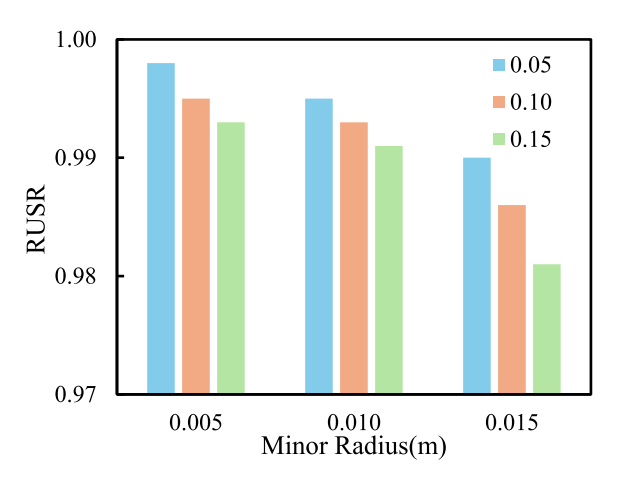


Fig. 34. RUSR calculation results under surface crack.

damage in engineering practice. Although they may not be as severe in terms of propagation as through-thickness cracks, once they reach a certain depth and length, they can still significantly weaken the ultimate strength of a jacket platform.

In this study, crack size parameters are employed to represent the structural integrity level and the degree of damage. The primary objective is to develop a multiscale finite element model for defect analysis and to verify whether the proposed modeling approach can capture the influence of structural defects such as cracks. Therefore, the structural material is simplified as conventional structural steel, without explicitly considering the enhanced resistance to laminar tearing provided by Z-direction performance steel (lamellar tearing resistant steel), which is commonly used in critical welded joints and thick plates. This simplification may lead to conservative estimates of ultimate strength, since in practical applications Z-direction performance steel improves resistance to laminar tearing and related failure mechanisms.

3.3.3. Mechanical dent

Mechanical dent defects were introduced at the main leg of the jacket platform, as shown in Fig. 35, to investigate their influence on the residual ultimate strength of the platform. A beam-solid model was used to simulate the structure containing the mechanical dents. Dents of identical dimensions were placed at both the upper and lower locations of the main leg, as indicated in the figure, to study the effect of dent location on the ultimate strength. In addition, the depths of the mechanical dents are assumed to be 0.25 m, 0.35 m, and 0.45 m, respectively, to investigate the effect of dent depth on the ultimate strength. In practical engineering, dents are often directional, a factor frequently overlooked in previous studies. To assess this aspect, the opening direction of the dent at the lower location was set to 0° and 90°, respectively, in order to evaluate the effect of dent orientation on structural performance.

The load-bearing capacity curves of the jacket platform are shown in Fig. 36, and the corresponding RUSR results are presented in Fig. 37. Overall, the residual ultimate strength of the platform decreases progressively as the dent depth increases. Taking the upper dent location as an example, when the dent depth reaches 0.45 m, the residual ultimate strength drops to approximately 78.9 % of that of the intact platform, indicating a significant strength reduction. Comparing the results between the upper and lower dent positions reveals that, under the same dent parameters, the lower-positioned dents lead to a more pronounced reduction in strength. This indicates that the closer the defect is to the bottom—where the jacket structure bears the main loads—the greater its impact on the overall structural performance. Additionally, a comparison of the results for different dent opening directions shows that the orientation of the dent has a considerable effect on the ultimate strength. Dents with identical parameters oriented in the 90° direction result in

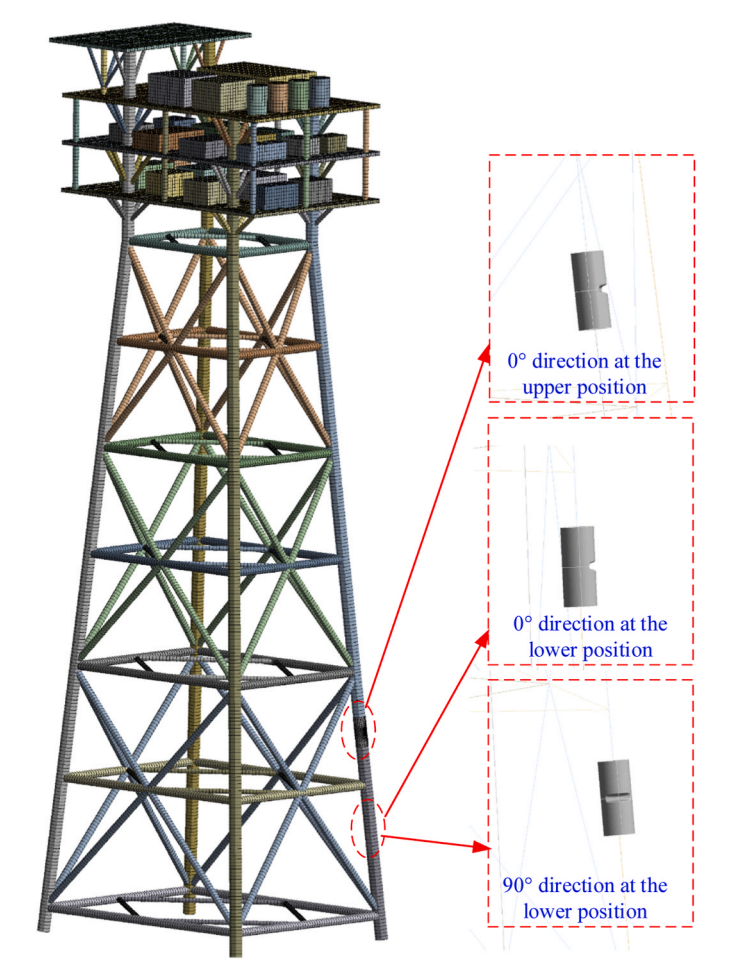


Fig. 35. Mechanical dent model.

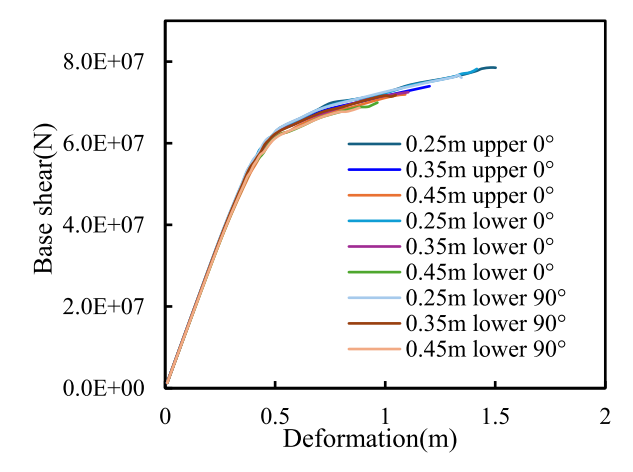


Fig. 36. Load-bearing capacity curve under mechanical dent.

more severe strength degradation. Therefore, in practical engineering applications, in addition to considering the geometric size of the dent, its orientation should also be taken into account to accurately assess its structural impact.

4. Conclusion

This work proposes a digital twin model calculation method for aging jacket platforms. Developed within the framework of DHE, the model enables efficient analysis of field-acquired data, thereby

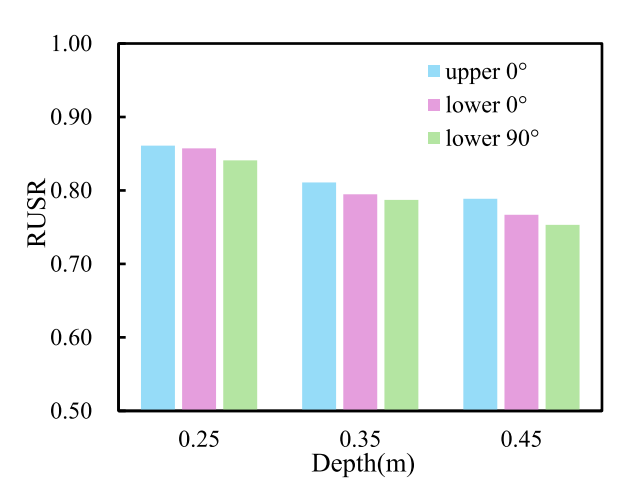


Fig. 37. RUSR calculation results under mechanical dent.

facilitating effective computation of environmental loads and the residual ultimate strength of the structure to support near real-time structural health monitoring. Tailored solutions are proposed for both environmental loads and the structural defects of aging jacket platforms to enhance the timeliness of digital twin computations. The main conclusions of this study are as follows.

- (1) In terms of environmental load calculation, dedicated schemes for wind, wave, and current loads are proposed. A wind load calculation method based on the construction of a Kriging surrogate model is introduced, which addresses the issues of low accuracy in formula-based calculations—particularly their inability to capture the variation with wind direction—and the inefficiency of CFD methods. This approach enables rapid wind load computation while ensuring accuracy. Wave and current loads are accurately calculated using Morison equation in combination with wave theories and current velocity profiles. By adjusting the parameters of environmental loads, the proposed method allows for near real-time and efficient calculation under different operating conditions. This not only makes near real-time updates of the digital twin model feasible but also provides essential support for emergency decision-making under extreme environmental conditions.
- (2) In terms of residual ultimate strength assessment for aging jacket platforms, a multi-scale finite element analysis-based method is proposed. Following the multi-scale finite element concept, the approach leverages the high computational efficiency of macrolevel beam-element models and the capability of refined local models to incorporate structural defects. A numerical model of the jacket platform is thus established by combining the macroscale global model with localized refined models, enabling the introduction of structural defects. This significantly reduces the number of elements required while maintaining a balance between accuracy and efficiency. Furthermore, specific modeling approaches are proposed for different types of structural defects, including uniform corrosion, pitting, fatigue cracks, and mechanical dents. Using a case study of an aging jacket platform, local structural defects are introduced at designated locations. The results demonstrate that the multi-scale finite element model can effectively transfer the information from localized models into the macro-scale model, which is ultimately reflected in the residual ultimate strength calculations, thereby validating the effectiveness of the proposed method.

In conclusion, the proposed method significantly enhances computational efficiency, enabling near real-time analysis and processing of monitoring data, and thereby providing a comprehensive solution for

the digital twin modeling of aging jacket platforms. At the same time, it establishes a foundation for real-time health diagnosis, prediction, and maintenance decision-making of aging jacket platforms within the DHE framework

The method proposed in this study still has certain limitations and shortcomings in practical engineering applications. Future work should focus on further improvements and refinements in the following aspects.

- (1) Establishment of a complete digital twin system. The focus of this study is the development of a computational method for environmental loads and residual ultimate strength to support a digital twin model. In future research, physical testing should be conducted, and systems for field data acquisition, transmission, and communication should be implemented. Combined with the method proposed in this work, real-time simulation and analysis of the data can be performed to realize a complete, closed-loop digital twin for aging jacket platforms, providing support for real-time structural health assessment and life-extension decision-making.
- (2) Development of experimental validation for the digital twin model. Digital twin approaches need to reflect responses under real-world conditions; therefore, it is necessary to develop experimental validation techniques for the digital twin model. In future work, feasible validation schemes for the digital twin approach should be designed. This may involve constructing scaled models or monitoring the structural mechanical responses of actual aging jacket platforms to obtain response data, which can then be used to further calibrate and validate the proposed method.
- (3) Validating the rationality of the load calculation method using real sea-state data. At present, the environmental load parameters adopted in the calculations are represented in the form of multiple directions and multiple levels, which still differ to some extent from measured data. Future work should incorporate real monitoring data from field conditions to obtain parameter time series, enabling modeling and analysis of real-time recorded environmental parameters. This will further extend the applicability of the proposed method and verify its feasibility.
- (4) Further refinement of the local detailed model is required. In future experimental validation, more realistic material properties of jacket structures and the characteristics of local detailed models should be taken into account. During modeling, specific enhanced material properties—such as those of Z-direction performance steel—should be incorporated to analyze their influence on the calculated ultimate strength. This will enable the development of more detailed microscale models, thereby facilitating deeper investigation into the behavioral patterns of ultimate strength and enhancing the rigor of engineering applications.

CRediT authorship contribution statement

Keyang Liu: Writing – original draft, Visualization, Validation, Methodology, Formal analysis, Conceptualization. **Yuanchang Liu:** Supervision, Writing – review & editing. **Baoping Cai:** Writing – review & editing. **Jeom Kee Paik:** Supervision.

Declaration of competing interest

The authors declare that they have no known competing financial interests or personal relationships that could have appeared to influence the work reported in this paper.

Acknowledgments

The authors received no specific funding for this work.

References

- Ali, L., Khan, S., Bashmal, S., Iqbal, N., Dai, W.S., Bai, Y., 2021. Fatigue crack monitoring of T-Type joints in steel offshore oil and gas jacket platform. Sensors 21 (9).
- Alizadeh, A., Daghigh, M., Bali, M., Golpour, H., Kazeminezhad, M.H., 2024. A framework for implementing structural integrity management of an aging fixed offshore platform using wave modeling for risk-based underwater inspection provision. Ocean Eng. 309.
- Asgarian, B., Zarrin, M., Sabzeghabaian, M., 2019. Effect of foundation behaviour on steel jacket offshore platform failure modes under wave loading. Ships Offshore Struct. 14 (6), 570–581.
- Bai, Y., Kim, Y., Yan, H.B., Song, X.F., Jiang, H., 2016. Reassessment of the jacket structure due to uniform corrosion damage. Ships Offshore Struct. 11 (1), 105–112.
- Chiu, R., Yu, W., 2023. Heterogeneous beam element for multiscale modeling of non-prismatic composite beam-like structures. Int. J. Solid Struct. 285.
- Cui, M.X., He, K.H., Wang, F., Paik, J.K., 2025. Human digital healthcare engineering for enhancing the health and well-being of seafarers and offshore workers: a comprehensive review. Systems 13 (5).
- Duan, W.X., Tan, P., Paik, J.K., 2024. Enhancing safety and resilience of ageing land-based LNG Tank structures through digital healthcare engineering: a feasibility assessment in seismic environments. Ships Offshore Struct. https://doi.org/10.1080/17445302.2024.2428229.
- El-Din, M.N., Kim, J., 2014. Sensitivity analysis of pile-founded fixed steel jacket platforms subjected to seismic loads. Ocean Eng, 85, 1–11.
- Fadzil, N.M., Muda, M.F., Shahid, M.D.A., Mustafa, W.A., Mohd, M.H., Paik, J.K., Hashim, M.H.M., 2024. Digital healthcare engineering for aging offshore pipelines: a state-of-the-art review. Ships Offshore Struct. https://doi.org/10.1080/ 17445302.2024.2424330
- Huang, S.N., Sun, Q.H., Bai, W., Guo, X., Dai, J.W., Ma, C., 2025. Seismic performance of aged jacket platforms subjected to onshore and offshore earthquakes. Ocean Eng. 338.
- Jayasinghe, S.C., Mahmoodian, M., Sidiq, A., Nanayakkara, T.M., Alavi, A., Mazaheri, S., Shahrivar, F., Sun, Z., Setunge, S., 2024. Innovative digital twin with artificial neural networks for real-time monitoring of structural response: a port structure case study. Ocean Eng. 312.
- Ji, C.Y., Xue, H.Z., Shi, X.H., Gaidai, O., 2016. Experimental and numerical study on collapse of aged jacket platforms caused by corrosion or fatigue cracking. Eng. Struct. 112, 14–22.
- Jia, Z.G., Dai, S., Fan, Z.L., Jia, S., Su, X., Wang, Y.L., 2025. Model updating method for offshore jacket platforms using improved DNN and OOA considering non-uniform corrosion and structural responses. Structural Health Monitoring-an International Journal. https://doi.org/10.1177/14759217241309319.
- Karimi, H.R., Karamzadeh, N.S., Gholami, E.O.R., 2025. Assessing the behavior of fixed offshore jackets in failure condition, evaluation in ultimate State to improve structural safety. Eng. Rep. 7 (5).
- Karimi, H.R., KaramZadeh, N.S., Golami, E.O.D.R., 2017. Effect of elevational and member damage on jacket strength: sensitivity and reliability review of South Pars phase-20 jacket, using push-over analysis. Ocean Eng. 143, 209–216.
- Kim, H.J., Paik, J.K., 2025. A digital twin model within the framework of a digital healthcare engineering system for aging containership hull structures. Ships Offshore Struct. https://doi.org/10.1080/17445302.2025.2505827.
- Lee, J.-H., Nam, Y.-S., Kim, Y., Liu, Y., Lee, J., Yang, H., 2022. Real-time digital twin for ship operation in waves. Ocean Eng. 266.
- Leng, J., Chen, Z., Ren, C., Zhang, J., Zhang, J., 2025. Online prediction of crack propagation of jacket platform based on PSO-DBN. Ships Offshore Struct. 1–16.
- Liang, Y.J., Lu, Y.J., Gao, D.X., Wang, Z.S., 2022. Approximation optimal vibration control with applications to jacket offshore platforms with nonlinear dynamic characteristics. Int. J. Control Autom. Syst. 20 (2), 507–514.
- Lin, H., Yang, L., Moiseevish, U.A., Han, C., Luan, H., Chen, G., 2022. Failure analysis and safety assessment of offshore platform under different ship collision scenarios by Numerical simulation. J. Perform. Constr. Facil. 36 (6).
- Lin, H., Zhang, S., Uzdin, A.M., Wei, L.C., Fan, Q., Yang, L., 2025. Numerical study on hydrodynamic characteristics, wave forces and dynamic responses of offshore jacket platform under tsunami-like solitary waves. Ocean Eng. 318.
- Liu, H.B., Chen, G.M., Sun, L.P., Zhu, B.R., Huang, A., Zhao, Y.P., 2021. Assessment of wind-induced responses for offshore jacket platforms based on high frequency force balance tests. Int. J. Oil Gas Coal Technol. 26 (4), 357–381.
- Mujeeb-Ahmed, M.P., Paik, J.K., 2021. Quantitative collision risk assessment of a fixedtype offshore platform with an offshore supply vessel. Structures 29, 2139–2161.

- Othman, N.A., Mohd, M.H., 2024. Response of the offshore jacket platform at its ultimate strength under operating and extreme loads: a Malaysian waters case study. Ships Offshore Struct. 19 (11), 1805–1826.
- Paik, J.K., 2024. Enhancing safety and sustainability through digital healthcare engineering. Marine Technology. The Society of Naval Architectures and Marine Engineers, Alexandria, VA, USA, April, pp. 34–40.
- Punurai, W., Azad, M.S., Pholdee, N., Bureerat, S., Sinsabvarodom, C., 2020. A novel hybridized metaheuristic technique in enhancing the diagnosis of cross-sectional dent damaged offshore platform members. Comput. Intell. 36 (1), 132–150.
- Raheem, S.E.A., 2014. Study on nonlinear response of steel fixed offshore platform under environmental loads. Arabian J. Sci. Eng. 39 (8), 6017–6030.
- Ruan, W.D., Qi, K.F., Han, X.X., Sun, B., Gao, X.F., Li, J.T., 2023. Multi-scale coupling numerical modeling of metallic strip flexible pipe during reel-lay process. Ocean Eng. 283.
- Shehata, M., Abdelnaeem, M., Mokhiamar, O., 2022. Performance enhancement of a tuned mass damper for vibration suppression of an offshore jacket platform utilizing a novel metaheuristic optimization technique. Ocean Eng. 263.
- Sindi, A., Kim, H.J., Chaves, I.A., Paik, J.K., 2025. Effect of corrosion wastage on the limit states of monopile-type offshore wind turbines under combined wind and rotor blade rotation. Materials and Corrosion-Werkstoffe Und Korrosion 76 (6), 790–801.
- Sindi, A., Kim, H.J., Yang, Y.J., Thomas, G., Paik, J.K., 2024. Advancing digital healthcare engineering for aging ships and offshore structures: an in-depth review and feasibility analysis. Data-Centric Engineering 5.
- Tabeshpour, M.R., Erfani, M.H., Sayyaadi, H., 2020. Challenges in calculation of critical buckling load of tubular members of jacket platforms in finite element modeling. J. Mar. Sci. Technol. 25 (3), 866–886.
- Tatum, S., Allmark, M., Frost, C., O'Doherty, D., Mason-Jones, A., O'Doherty, T., 2016.
 CFD modelling of a tidal stream turbine subjected to profiled flow and surface gravity waves. International Journal of Marine Energy 15, 156–174.
- Tian, X.J., Wang, Q.Y., Liu, G.J., Liu, Y.X., Xie, Y.C., Deng, W., 2019. Topology optimization design for offshore platform jacket structure. Appl. Ocean Res. 84, 38–50.
- Wahab, M.M.A., Kurian, V.J., Liew, M.S., Kim, D.K., 2020. Condition assessment techniques for aged fixed-type offshore platforms considering decommissioning: a historical review. J. Mar. Sci. Appl. 19 (4), 584–614.
- Wang, B., Sun, W., Wang, H., Xu, T., Zou, Y., 2024. Research on rapid calculation method of wind turbine blade strain for digital twin. Renew. Energy 221.
- Wang, R.H., Zou, X., Dou, P.L., Fang, Y.Y., Luo, G.E., 2015. Asme, 2015. multi-Scale investigation on residual strength of jacket platform with fatigue crack damage. In: Proceedings of the Asme 34th International Conference on Ocean, vol. 3. Offshore And Arctic Engineering.
- Westin, C., A. Irani, R., 2025. Framework for a physics-based digital twin of a towed cable-body system. Ocean Eng. 328.
- Xie, Y.H., Kim, H.J., Yin, Y.C., Liu, K.Y., Smith, T., Paik, J.K., 2025. Enhancing the safety and sustainability of aging jacket-type offshore wind turbines in extreme weather conditions through digital healthcare engineering: a literature review. Ships Offshore Struct. https://doi.org/10.1080/17445302.2025.2502868.
- Yang, Y., Wu, Q.J., He, Z., Jia, Z.Y., Zhang, X.W., 2019. Seismic collapse performance of jacket offshore platforms with time-variant zonal corrosion model. Appl. Ocean Res. 84, 268–278.
- Yang, Y., Xu, T.Y., Guo, J.L., He, Z., Ma, H.B., 2021. Length strength reserve assessment on pitting-corroded jacket offshore platforms based on the modified generalized constitutive model. Thin-Walled Struct. 169.
- Yang, Y., Ying, X.H., Guo, B.X., He, Z., 2017. Collapse safety reserve of jacket offshore platforms subjected to rare intense earthquakes. Ocean Eng. 131, 36–47.
- Zhang, B., Shang, Z.Q., Wang, T., Wang, Z., 2020. Hydrodynamic load analysis and experimental study of grouting clamp under wave and ocean current. J. Mar. Sci. Eng. 8 (7).
- Zheng, Z.Q., Chang, Z.Y., Zhao, L., 2024. Mitigating jacket offshore platform vibration under wave loadings utilising nonlinear energy sinks. Ships Offshore Struct. 19 (9), 1323–1331.
- Zhou, B., Han, X.S., Tan, S.K., 2014. A simplified computational method for random seismic responses of a jacket platform. Ocean Eng. 82, 85–90.
- Zhu, L., Wang, X.G., Guo, K.L., Ma, B., Amer Soc Mechanical, E., 2020. Numerical studies on dynamic behavior of tubular pipes under repeated impacts. In: Proceedings of the Asme 39th International Conference on Ocean, 2A. Offshore And Arctic Engineering, OMAF2020.
- Zou, Y., Liu, Y., Chen, Z., Liu, J., Chen, J., Chen, M., Lv, P., Duan, H., Li, H., 2024. Data driven digital twin system for the cross-domain vehicle. Ocean Eng. 311.